

POLITECNICO DI TORINO

Master Degree in Environmental and Land Engineering

Academic Year 2025/2026

September 2026

Water resources and plant health in greenhouse-grown tomato plants

Supervisor:

Stefania Tamea

Cosupervisors:

Cum Federico

Demarchi Danilo

Shahmohammadi Amirarsalan

Candidate:

Marcella Brignone

Table of contents

Abstract 2
Chapter 1 Introduction 3
Chapter 2 Background 5
2.1 The soil-plant-atmosphere continuum 5
2.2 The water balance of the growing medium 7
2.3 Electrical stem impedance 8
2.3.1 Electrical impedance in tomato 9
Chapter 3 Materials and methods 11
3.1 Experimental design, dataset and measurement system 11
3.2 Data analysis 12
3.3 Water balance 14
3.3.1 From soil water potential to water content 15
3.3.2 Reference evapotranspiration 17
3.3.3 The AgrHyd water balance model 21
3.3.4 Plant selection and comparison 22
Chapter 4 Results 24
4.1 Dataset overview and behavioural classes 24
4.2 Stem-frequency analysis 25
4.2.1 Behaviour and correlation of the stem frequency 25
4.2.2 Form and timing of the frequency-SWP relationship 31
4.3 Water balance 31
Chapter 5 Discussion 37
5.1 The stem frequency as a water-stress indicator 37
5.2 The drainage of gravitational water and the domain of validity of the model 39
5.3 The two approaches compared 40
5.4 Limitations and future developments 42
Chapter 6 Conclusions 43
References 45
Appendices 48
Appendix A Code 48

Appendix B Model parameters and crop coefficient grid 51
Appendix C Reference evapotranspiration 52
Appendix D Simulated versus observed water content, all plants 53
Acknowledgements 57

Abstract

Agriculture is exposed to the effects of climate change, which has altered water availability and the frequency of drought. Monitoring the water status of crops, and modelling the exchanges between soil, plant and atmosphere, has therefore become increasingly necessary to support sustainable farming. This thesis examines the response to water stress of tomato plants grown in a greenhouse, combining experimental data with modelling, with the aim of validating the model estimates and providing an interpretive basis for the observations. The water status of the plants is examined from two complementary sides. The first rests on a measurement taken on the plant itself, the electrical impedance of the stem, recorded continuously as a frequency. The frequency follows the soil water potential in the plants under deficit, with a strong correlation that persists once the evaporative demand of the atmosphere is removed, while it is absent in the irrigated plants. The signal therefore acquires diagnostic meaning specifically under stress, and it remains informative beyond the range in which the soil water potential sensor saturates. The second side rests on a water balance model, used to reconstruct the water content of the substrate and to compare it with the content derived from the measured potential through the retention curve. With the crop coefficient determined within the FAO-56 reference range, the model reproduces the observed drying of the plants that begin the monitoring within the slow-release range of the substrate but departs systematically from it in the plants that begin at field capacity. A mass balance attributes the departure to the drainage of gravitational water, which leaves the root zone without passing through the plant and which the model does not account for. The analysis thus delimits the range of conditions over which the water balance can be validated against the potential measurements. The comparison of the two approaches shows that they describe the same drying process from opposite ends of the soil-plant-atmosphere continuum, and that their limitations are complementary: the measurement in the substrate is reliable only within a narrow window of potential, while the measurement on the plant remains informative beyond it. The two converge under stress, where both respond to the shortage of water. Taken together, rather than singly, the two approaches allow water stress to be followed over the whole course of the drying and contribute to the development of tools for a more efficient use of water in agriculture without loss of yield.

Chapter 1 Introduction

Agriculture accounts for the largest share of the fresh water withdrawn worldwide, and the pressure on that share is increasing (FAO, 2021; IPCC, 2022). Rising temperatures, more frequent droughts and the growing competition for water between agricultural, industrial and domestic uses make it increasingly costly to irrigate by habit or on a fixed schedule, rather than according to the actual need of the crop (IPCC, 2022). In the Mediterranean region, where the summer deficit between rainfall and evaporative demand is structural, the water applied to a crop has become a resource to be allocated with care (IPCC, 2022, Ch. 13). The efficiency of its use is addressed directly by the Sustainable Development Goals, and in particular by Goal 6 on clean water and sanitation, whose target 6.4 calls for a substantial increase in water-use efficiency across all sectors and for a sustainable withdrawal of fresh water (United Nations, 2015). Since the water supplied to a crop determines the yield it can sustain, the same question also bears on Goal 2 on food security, which depends on producing more with the water that remains available (United Nations, 2015).

A greenhouse shelters the crop from rainfall, so that the whole of its water supply passes through irrigation, and the atmospheric conditions inside it differ from those outside, with attenuated radiation, reduced air movement and a modified vapour pressure deficit. When the crop is grown in containers filled with an artificial substrate, the volume of water available to the roots is limited to the volume of the container, and the water status of the medium can change over the course of a few days. These conditions make the response of the crop to a deficit rapid, and they make the decision of when to irrigate, and how much water to apply, correspondingly consequential for the plant.

The practical problem behind irrigation management is knowing when a crop is beginning to suffer from a shortage of water, and two families of methods address it from opposite ends of the system that connects the soil, the plant and the atmosphere. The first describes the availability of water in the medium, either by measuring it with sensors or by simulating it with a water balance that subtracts the evapotranspiration from the water stored in the root zone; this gives an estimate of the depletion in depth of water, and so of the amount to be restored. The second observes the plant itself, through a signal that changes as its tissues lose water; this reports the condition of the plant, and so the moment at which a deficit becomes physiologically relevant. Each family carries different advantages and limitations, that are analyzed in this work.

Both approaches are examined here on the same plants and over the same drying cycles, using the material of a monitoring experiment carried out on greenhouse-grown tomato plants in which stem electrical impedance, read as the frequency of a relaxation oscillator, was recorded continuously alongside the soil water potential and the greenhouse microclimate, on plants kept under regular irrigation and on plants left to dry. On this dataset the stem frequency is analysed as an indicator of the water condition of the plant, and the water content of the substrate is simulated with the AgrHyd water balance model, driven by a reference evapotranspiration computed for the greenhouse environment, and compared with the water content derived from the measured potential.

A series of objectives are carried out starting from this configuration. The first is to establish whether the stem frequency reflects the water status of the plant, under which conditions it does so, and how its response separates from the influence of the atmospheric demand. The second is to determine how accurately a water balance model built on the FAO-56 procedure reproduces the drying of a container substrate, and to identify the processes that govern its agreement with the observations. The third is to compare what the two approaches describe, in

order to establish the range over which each of them is informative and to assess what their joint use adds to the monitoring of water stress.

Chapter 2 reviews the background of the two approaches, covering the soil-plant-atmosphere continuum and evapotranspiration, the water balance and the response of a crop to water stress, and the electrical impedance of plant tissue as a measure of water status. Chapter 3 describes the experimental setup and the dataset, the processing and the statistical methods applied to the measurements, and the construction of the water balance, from the conversion of the soil water potential into water content to the determination of the crop coefficient and the selection of the plants. Chapter 4 presents the results of the two approaches. Chapter 5 discusses them, examining the stem frequency as a stress indicator, the drainage process that governs the agreement of the model and its domain of validity, the comparison between the two approaches and the limitations of the study. Chapter 6 draws the conclusions and outlines the developments that would follow from them.

Chapter 2 Background

2.1 The soil-plant-atmosphere continuum

Water moves from the growing medium to the atmosphere along a continuous path that passes through the plant. The medium supplies water to the roots, the vascular tissue conducts it to the leaves, and the leaves release it to the air as vapour through the stomata. Although the path crosses phases and tissues of different nature, the flow is governed throughout by a single quantity, the water potential, and proceeds from regions of higher to regions of lower potential.

The water potential expresses the energy state of water relative to free water at reference conditions (Taiz and Zeiger, 2002) and is conventionally negative in an unsaturated medium. In a growing medium the dominant component is the matric potential, which arises from the adsorption of water on particle surfaces and from capillary forces in the pores: the drier the medium, the more tightly the remaining water is held and the more negative the potential becomes. Within the plant, the potential of the xylem sap is lowered further by the tension generated at the evaporating surfaces of the leaves. In the atmosphere the potential is lower still by several orders of magnitude, since it depends on the vapour pressure of the surrounding air.

The gradient along this path is therefore steep and directed outward, from the medium towards the atmosphere. Its magnitude is not, however, the only quantity that determines the flow, which is limited by the resistances encountered along the way. The most important of these are the resistance to water movement in the medium towards the root surface, the resistance at the soil-root interface and within the root tissue, the axial resistance of the xylem, and the stomatal resistance at the leaf surface. Of these, the stomatal resistance is the only one under active control of the plant, and its regulation is the principal mechanism by which transpiration is adjusted to the water available (Taiz and Zeiger, 2003; Raviv et al., 2019).

The consequence is that the state of the plant is not determined by the water content of the medium alone. When water is abundant, the potential of the medium is high and nearly constant, the resistances are low, and transpiration proceeds at the rate imposed by the evaporative demand of the atmosphere. As the medium dries, its potential falls and the resistance to water movement towards the roots increases, so that the supply becomes progressively less able to match the demand. The plant responds by closing the stomata, which lowers transpiration below its potential rate. From this point the flow is governed by the supply rather than by the demand, and the plant is in a condition of water stress (Taiz and Zeiger, 2003; Allen et al., 1998).

The same drying process therefore leaves a trace at both ends of the continuum. In the medium it appears as a decrease of the water potential and of the water content. In the plant it appears as a reduction of transpiration and as changes in the water status of the tissues. The two are related, but they are not the same quantity, and they do not necessarily vary in step: the medium acts as a reservoir whose state changes slowly, while the plant responds within the day to the evaporative demand and to its own hydraulic regulation.

This distinction underlies the approach followed in this work. The condition of the plants is examined from both ends of the continuum: from the medium, through the water potential recorded by the substrate probes and through the water balance of the pot, and from the plant, through the electrical impedance of the stem. The two measurements describe the same drying process, but they are taken at different points of the path and are subject to different limitations, which are the subject of the chapters that follow.

Evapotranspiration is the transfer of water from a cropped surface to the atmosphere as vapour. It combines two processes that occur simultaneously and are difficult to separate in practice: evaporation, by which water is lost from the surface of the growing medium, and transpiration,

by which water taken up by the roots is released through the stomata of the leaves. The two respond to the same atmospheric conditions but draw on different parts of the system, and their relative weight changes as the crop develops: evaporation prevails when the canopy is sparse and the medium is exposed, transpiration when the canopy has closed and intercepts most of the incoming radiation.

The rate of evapotranspiration is determined by the energy available to vaporise water, by the capacity of the air to remove the vapour produced, and by the properties of the surface. The first depends principally on net radiation, the second on the vapour pressure deficit and on wind speed, and the third on the reflectance, roughness and stomatal behaviour of the crop. Since the atmospheric terms are common to any surface exposed to the same conditions, while the surface terms are specific to each crop and to its stage of development, it is convenient to separate the two contributions rather than to treat each crop independently.

This is the basis of the reference evapotranspiration approach adopted in the FAO-56 procedure (Allen et al., 1998). The reference evapotranspiration ET0 is defined as the evapotranspiration of a hypothetical grass surface of fixed height, albedo and surface resistance, well-watered and completely shading the ground. Because its surface properties are fixed, ET0 depends only on the atmospheric conditions and expresses the evaporative demand of the climate. The evapotranspiration of an actual crop is then obtained from ET0 through coefficients that account for the difference between that crop and the reference surface:

$$ET_C = K_C \cdot K_S \cdot ET_0 \tag{2.1}$$

The crop coefficient Kc represents the ratio between the evapotranspiration of the crop under standard conditions, that is with no limitation of water supply, and the reference evapotranspiration. It incorporates the differences in canopy height, albedo, surface resistance and exposed soil surface, and it varies through the growing season as the canopy develops. In the FAO-56 procedure it is described as a piecewise function of four stages: an initial value while the canopy is sparse, a rise during the development stage, a plateau at the maximum value through the mid-season, and a decline as the crop senesces. The tabulated values refer to a complete cycle under standard field conditions and are meant to be adjusted to the local climate and to the actual duration of the stages.

The water stress coefficient Ks accounts for the reduction of evapotranspiration when the water available in the root zone is no longer sufficient to meet the demand. It equals unity while the water content remains above a threshold, below which it decreases as the reservoir is depleted, reaching zero at the wilting point. The threshold is defined as a fraction of the total available water, the depletion factor, which depends on the crop and on the evaporative demand: a crop can deplete a larger fraction of the reservoir before suffering stress when the demand is low, and a smaller fraction when it is high. The two coefficients therefore describe distinct effects, Kc the potential evapotranspiration of a developed canopy and Ks its reduction under limited supply, and they enter the calculation as independent factors.

The reference procedure was established for open field conditions, and its application to protected environments requires attention. A greenhouse alters the terms that determine evapotranspiration: the cover reduces the incoming solar radiation, the enclosure lowers wind speed to values well below those of the open air, and the confined volume modifies the vapour pressure deficit. The reference evapotranspiration computed from external climatic data therefore overestimates the demand inside the structure, and the procedure must be adapted to

the conditions of the enclosure. The adaptation adopted in this work is described in Section 3.3.2.

2.2 The water balance of the growing medium

The water content of a volume of growing medium changes according to the balance between the water that enters and the water that leaves it. Over a given interval of time,

$$\Delta S = P + I - ET_C - D - R \tag{2.2}$$

where ΔS is the change in stored water, P the precipitation, I the irrigation, ETc the evapotranspiration, D the drainage below the root zone and R the surface runoff. The terms are usually expressed as depths of water over the surface considered, so that a water content can be converted into millimetres by multiplying it by the depth of the layer.

Depending on the context, some terms can be neglected. Under cover, such as in a greenhouse, precipitation is absent. In a container of limited surface, runoff is negligible, and the medium is bounded below, so that drainage leaves through the holes at the base rather than percolating into deeper layers. When irrigation is withheld, the balance reduces to the loss terms alone, and the change in storage is determined by evapotranspiration and drainage.

The water stored in the medium is not entirely available to the plant. The balance is therefore described in terms of a reservoir bounded by two limits (Allen et al., 1998). The upper limit is the water content retained against gravity once the excess has drained, and the lower limit is the water content below which the plant can no longer extract water, conventionally the content at a potential of -1500 kPa. The difference between the two is the total available water of the root zone, and the models of water balance follow its depletion over time.

The upper limit is the field capacity, the water content retained against gravity once the excess has drained. The water held above it is gravitational water: it occupies the largest pores, is retained by forces weaker than gravity, and drains downward without being available to the plant.

The removal of gravitational water is gradual, as the drainage rate depends on the unsaturated hydraulic conductivity, which in growing media falls abruptly within the same narrow range of potential over which most of the water is released (Londra et al., 2018). A medium that has just been wetted therefore continues to lose water by gravity for a period that can extend over more than one day, during which the decrease of its water content is only in part attributable to the plant.

In models of water balance operating on a daily time step, at each step the storage is updated by adding the inputs and subtracting the losses, the evapotranspiration is computed from the reference evapotranspiration and the crop coefficients, and the water content is constrained between the two limits. The excess above the upper limit is removed as drainage, usually within the same step, so that the simulated medium is never held in an oversaturated condition. This treatment is adequate when the interest lies in the depletion of the reservoir by the crop, and it is the basis of the model applied in this work, described in Section 3.3.3.

Water stress arises when the water available to the plant is no longer sufficient to meet the demand imposed by the atmosphere. It is a progressive condition: as the medium dries, its potential falls and the resistance to water movement towards the roots increases, so that the supply becomes gradually less able to sustain the transpiration required. The plant experiences

stress when this imbalance forces it to reduce transpiration below the rate that the evaporative demand would otherwise impose.

The first response is the closure of the stomata (Taiz and Zeiger, 2002). By increasing the stomatal resistance, the plant limits the loss of water vapour, at the cost of also restricting the entry of carbon dioxide and therefore of reducing photosynthesis. As the stress deepens, the loss of turgor reduces cell expansion and slows the growth of new tissue, which is among the processes most sensitive to a shortage of water. A prolonged or severe deficit affects the water status of the tissues more widely, with a decrease in their water content and, in some species, an accumulation of solutes that lowers the osmotic potential and allows water to be retained at more negative potentials.

The condition of the plant under stress can be assessed at different points of the continuum, and the choice of indicator determines what is measured. The water potential of the medium, obtained from tensiometers or from granular matrix sensors, describes the state of the reservoir from which the plant draws, and is an indirect indicator: it reports the availability of water rather than the response of the plant. The leaf water potential, measured with a pressure chamber, reports the tension in the xylem and is closer to the state of the plant, but it requires a destructive and discontinuous measurement, which is difficult to automate for continuous monitoring. Indicators based on the plant itself, such as sap flow, stem or leaf variations in diameter, canopy temperature or the electrical properties of the tissues, respond to the internal water status and can be recorded continuously, at the cost of a less direct relation to the water potential and of a response that reflects the combined effect of several factors.

The measurement adopted in this work belongs to this last group. The electrical impedance of the stem responds to the water content of the tissues and to the concentration of ions in the cell sap, both of which change as the plant loses water, and it can be recorded continuously and without damage to the plant. Its principle and its relation to the water status are described in the following section.

2.3 Electrical stem impedance

The electrical impedance of a vegetal tissue reflects its cellular setup. The stem's tissue is composed of extracellular fluid where cells are immersed; each cell is made of a membrane, a wall and an intracellular fluid. From an electrical point of view, the plasmatic membrane behaves as a capacitor, and intra and extra cellular fluids act as a resistance. This equivalence leads to the representation of the vegetal tissue as an equivalent circuit. The reference model was proposed by Hayden et al. (1969) and subsequently expanded and applied to vegetal tissues by Zhang and Willison (1993).

The behaviour of impedance depends on the applied frequency signal: at low frequencies, the current flows mainly through the extracellular fluid, because the high capacitive reactance of the membrane opposes the flow; as the frequency increases, the reactance of the membrane decreases and the current flows through the intracellular fluid, at lower resistance, so that the overall tissue impedance decreases. Hence, the impedance spectrum is governed by the physical parameters of the cells (geometry, wall and plasmatic membrane properties, conductance of intra and extra cellular compartments) and that each element of the equivalent circuit has its physical meaning. (Sugiyama and Okajima, 2022).This mechanism explains the link between electrical impedance and water status in a plant, therefore it leads to the use of the parameter as an indicator of water stress.

Water scarcity modifies the electrical properties of the stem tissue acting on the extracellular conductive path. Since at medium-low frequencies the current mostly flows in extracellular fluid, because it's inhibited by the membrane to access intracellular fluid, and it only reaches it at higher frequencies, the extracellular compartment dominates the response, in the form of impedance, in the band of interest. The fluid is an ionic solution of which the volume and continuity of its flow influence the conduction: with dehydration, the volume diminishes and the paths shrink, so that the extracellular resistance increases, hence an increase in impedance is witnessed. Several studies confirm this phenomenon: in dehydrating leaves and stems, the extracellular fluid's resistance follows the decrease in water content, showing a negative correlation between the two parameters; in 1-hour long simulation of water stress condition, an increase of 25% in resistance was witnessed.

In addition, if the water stress condition is severe and prolonged, the membrane integrity is altered. This can lead to peroxidation of membrane lipids, compromising the structure of the membrane and consequently causing a leakage of ions, hence, a perturbation of the ionic balance between the compartments; a damaged membrane's capacity alters the spectrum of impedance. Consequently, the relationship between impedance and water status is monotone and can be interpreted in a quantitative way in a moderate stress condition, when the membranes are intact; under severe and prolonged water stress, opposing effects can be introduced because of the leakage of ions, hence the impedance is useful more as a qualitative indicator, rather than as a direct measure of water content.

Stem impedance is a state variable, as it depends on how much water, and therefore how much conductive ionic fluid, is present in the tissue between the electrodes at a given moment, not on how fast the sap moves through it. For this reason, it reports tissue water content rather than transpiration flow, which is why electrical and dielectric measurements are routinely used to estimate stem water content, with results that agree well with independent measures of plant water status. Transpiration still leaves its mark on the signal, though indirectly, and it accounts for the variation seen on a daily scale. The stem works as a water reservoir with its own capacitance: during the day, when transpiration outpaces the recharge supplied through the tissues, the stored water is drawn down and the impedance rises, while at night the reserve is refilled and the impedance falls again (Zweifel et al., 2001). What the diurnal cycle records is the day-to-day water storage state of the plant. The capacitance of this reserve also introduces a delay between the onset of transpiration and sap flux. The signal thus carries two timescales at once: a slow drift over days to weeks follows the average water status of the tissue, and ultimately the soil water supply; a faster circadian oscillation comes from the daily emptying and refilling of the reservoir.

2.3.1 Electrical impedance in tomato

Tomato (*Solanum lycopersicum*) is one of the most studied species through spectroscopy both because of its agronomic relevance and because the technique allows a non-destructive monitoring of several physiological aspects. As for water content status, recent studies documented the relationship discussed so far. On tomato plant stems, the phenomenon is confirmed and as previously described, severe dehydration deeply modifies the equivalent circuit. Besides this specific topic, impedance spectroscopy has been applied to tomato plants to diagnose not only its nutritional condition (phosphorus, nitrogen and potassium content), but also iron deficiency, detection of localized damage and the phase of maturation.

Most of the cited studies are based on spot or laboratory measurements, gained through spectroscopy analysis on detached tissues or at controlled water contents. A new strand of research at Polytechnic of Turin adopted *in vivo* and continuous monitoring: in a preliminary

study, frequency measures were adopted to distinguish abiotic stress from biotic stress, effectively identifying the plants in water stress condition. This thesis follows the latter and extends the research with prolonged monitoring of a wider number of tomato plants.

In the context of the study subject of this thesis, as described by Garlando et al. (A “Plant-Wearable System” for Its Health Monitoring by Intra- and Interplant Communication, 2023), the stem segment between the two inserted electrodes is connected as the impedance element in the feedback loop of a relaxation oscillator (LMC555), whose oscillation frequency is therefore governed by the stem's electrical impedance: therefore, the output parameter is the frequency (Hz) rather than the electrical impedance (Ohm). As shown in the same study, an inverse relationship exists between the two quantities, hence, a decrease in frequency corresponds to an increase in electrical impedance.

Chapter 3 Materials and methods

3.1 Experimental design, dataset and measurement system

The data analysed in this work were collected by the eLions group of the Department of Electronics and Telecommunications (DET, Politecnico di Torino), within a research project carried out with the Department of Agricultural, Forest and Food Sciences (DISAFA, Università di Torino). The experiment used stem impedance measurements to follow the response of tomato plants (*Solanum lycopersicum*) to biotic and abiotic stress. The measurement principle is a plant-wearable, low-cost and low-power method that reads the frequency of a relaxation oscillator in which a portion of the stem is part of the feedback loop, so that the oscillation frequency depends on the electrical impedance of the tissues and therefore on their water status. The frequency is thus used as an indicator of plant water stress. The approach follows the preliminary study of Cum et al. (2024) and extends it to a larger set of plants and conditions.

The trial was hosted in a greenhouse at Grugliasco (Turin, 293 m a.s.l., 45.06° N), a Venlo-type structure with a tempered glass cover and passive ventilation. The plants were grown in pots of 14 mm height filled with a commercial peat-based substrate (Turco Silvestro, TS3 line), whose physical properties and derived retention curve are described in Section 3.3.1. Measurements ran from 29th May 2024 to 16th December 2025. 14 measurement nodes were active at any given time, each hosting one plant in one of three conditions: healthy, abiotic stress and biotic stress. Abiotic stress was imposed by withholding water, whereas biotic stress was induced by inoculation with *Fusarium*, a soilborne pathogenic fungus. When a plant died it was replaced by another of the same species and developmental stage under the same condition, so that 87 plants were monitored in total. The plants were organised into seven successive clusters, each a group of plants followed over the same period between 2024 and 2025; the two clusters used for the water balance are described in Section 3.3.4.

Each node carried a set of sensors. The stem frequency was read by a relaxation oscillator built around an LMC555 timer with the stem in its feedback loop, active only during short measurement windows to limit the power draw. The soil water potential was measured by an Irrometer Watermark 200SS granular matrix sensor. Air temperature and relative humidity were recorded by a Texas Instruments HDC2080, and light intensity by an OPT3001. The analog stem-frequency signal was filtered by a high-pass stage and squared by a TLV7011 comparator before being counted. A Raspberry Pi Zero read the digital sensors over I²C and logged all channels, which were transmitted hourly over a LoRa link. The system was designed to operate without batteries, harvesting energy from miniature solar cells and a plant microbial fuel cell and storing it in supercapacitors.

The measurements were provided as a single chronologically ordered file and organised into a table in which each row is one timestamped reading of a given plant. Each node produced a reading once every 10 or 20 minutes, in alternation, throughout the monitoring period. Besides the timestamp, the recorded variables were the air temperature, the relative humidity, the raw Watermark resistance, the soil water potential, the stem frequency, and the identifiers of the node, of the plant and of its condition, together with any recorded symptoms. The monitored variables and their units are listed in Table 3.1. The conversion of the raw Watermark reading into soil water potential and the derivation of the further variables used in the analysis are described in Section 3.2.

Table 3.1. Variables recorded during the experiment.

Group	Variable	Unit
Environment	Air temperature	°C
	Relative humidity	%
Soil	Watermark resistance	kΩ
	Soil water potential	kPa
Plant	Stem frequency	Hz
	Node ID	-
	Plant ID	-
	Condition	-
	Symptoms	-

3.2 Data analysis

The raw dataset, provided as a chronologically ordered file, was imported and processed in Python. The timestamps were parsed to a standard datetime format, and the plant identifiers, initially stored as alphanumeric strings such as "node-1-grugliasco", were reduced to a unique numeric label to make grouping and sorting consistent. The records of each plant were then ordered in time, and a relative day index was defined, with the first day of a plant's record set as day one, so that plants monitored over different calendar periods could be compared on a common time axis. The time of day was also extracted from each timestamp for the sub-daily analyses, and every plant was assigned its experimental condition and its cluster from its identifier.

The soil water potential was measured indirectly with an Irrometer Watermark 200SS granular matrix sensor, read by a relaxation oscillator whose output frequency was first converted into the sensor resistance and then into soil water potential. The conversion from resistance to potential applies the temperature-compensated calibration of Shock (1998),

$$SWP = \frac{-3.213 \cdot R - 4.093}{1 - 0.009733 \cdot R - 0.01205 \cdot T} \quad (3.1)$$

where SWP is the soil water potential in kPa, R the sensor resistance in kΩ and T the soil temperature in °C. The calibration covers the range from 10 to 100 kPa, with linear extrapolation used below 10 and above 100 kPa, and a fully wet sensor corresponds to about 550 Ω.

The vapour pressure deficit was derived as an indicator of the evaporative demand of the air, which drives transpiration and evapotranspiration and provides the atmospheric variable against which the stem frequency was later compared. It was obtained from the air temperature and relative humidity following the FAO-56 procedure (Allen et al., 1998), with the saturation vapour pressure

$$e^{\circ}(T) = 0.6108 \cdot exp[\frac{17.27 \cdot T}{T + 237.3}] \quad (3.2)$$

the actual vapour pressure $e_a = e_s(T) \cdot RH / 100$, and the deficit $VPD = e_s - e_a$.

For the analyses carried out on a daily basis, and for the water balance, the sub-daily readings were aggregated into daily statistics for each plant, taking the daily mean together with the daily minimum and maximum of each variable.

Before analysis the data were screened for quality. The raw frequency series contain isolated spikes, single samples that depart from the local behaviour of the signal and are not physiological. These were identified with a robust criterion based on a moving median and the median absolute deviation (MAD): for each point a baseline was computed as the median of the frequency over a moving window of 36 hours, and the point was flagged as a spike when

$$| f_t - median_W(f) | > n \cdot MAD_W(f), \quad n = 8 \quad (3.3)$$

The median and the MAD were preferred to the mean and the standard deviation because, unlike the latter, they are not distorted by the very extreme values that the criterion is meant to detect, which makes the detection robust. The window of 36 hours was chosen so that the baseline follows the slow trend of the signal, due to growth and to stress, without following the daily cycle, so that the normal daily maxima are not mistaken for spikes, and the threshold of eight deviations flags only clear departures. For most plants the flagged fraction was below about one per cent, whereas a few plants showed a much higher fraction, up to about eleven per cent, concentrated in the first days of monitoring, when the sensor connection had not yet stabilised; for these plants the initial portion of the record was discarded rather than the flagged samples alone, so that genuine physiological variation in the rest of the series was preserved.

The Watermark sensor has a limited range of validity. It returns reliable values of soil water potential between 0 and about -239 kPa, and saturates at a full-scale value of about -1233 kPa; beyond the reliable limit the reported value may no longer correspond to the true potential of the substrate. Where the potential keeps decreasing in an orderly way its order is still preserved, so that rank-based analyses remain applicable, but where the reading flattens at the full-scale value it carries no further information. The two regimes were distinguished for each plant, and only the plants and periods whose potential stays within, or remains usefully ordered close to, the valid range were kept; analyses that require the absolute value of the potential, such as the water balance (Section 3.3), were confined to the valid range.

A few plants were set aside before analysis. Three plants (P33, P75 and P77) returned no usable frequency data and were excluded; one plant (P68) did not survive, and one record (P83) was found to duplicate that of another plant (P76), and both were removed. Two irrigated plants (P38 and P47) were retained but flagged, since their soil water potential remained pinned at the full-scale value while their frequency followed the pattern typical of irrigated plants, which points to a sensor fault rather than to real water stress. Finally, the stressed plants of cluster C4 never reached a genuine water-stress condition, their potential remaining above about -32 kPa throughout, and were not used where the development of stress was required.

The association between variables was assessed through correlation analysis, using two coefficients. The Pearson coefficient measures the strength of a linear association and is defined as

$$r_{xy} = \frac{\sum(x_i - \bar{x})(y_i - \bar{y})}{\sqrt{\sum(x_i - \bar{x})^2 \cdot \sum(y_i - \bar{y})^2}} \quad (3.4)$$

where x_i and y_i are the paired observations and $\bar{x}$, $\bar{y}$ their means; the numerator is their covariance and the denominator normalises it by their dispersions, so that r_{xy} lies between -1 and +1. The Spearman coefficient applies the same expression to the ranks of the data rather than to their values, and can be written as

$$\rho = 1 - \frac{6 \sum d_i^2}{n (n^2 - 1)} \tag{3.5}$$

where d_i is the difference in rank between the two variables for the i-th observation and n the number of pairs. By working on the order of the data instead of their magnitude, it measures a monotonic association and is insensitive to outliers and to departures from linearity. The coefficients reported in this work are Spearman's: the frequency-potential relationship is monotonic but not necessarily linear, the rank-based coefficient is robust to the isolated extreme values of the raw series, and, depending only on the order of the soil water potential, it remains usable beyond the absolute-value limit of the Watermark sensor. The Pearson coefficient was computed in parallel as a check and gave consistent results.

To separate the response of the frequency to the soil water potential from its response to the atmospheric demand, partial correlations were used. The partial correlation between two variables X and Y, with a third variable Z held constant, is

$$r_{XY \cdot Z} = \frac{r_{XY} - r_{XZ}\, r_{YZ}}{\sqrt{(1 - r_{XZ}^2)(1 - r_{YZ}^2)}} \tag{3.6}$$

obtained by removing from r_{XY} the correlation carried by Z and renormalising. With X the frequency, Y the soil water potential and Z the vapour pressure deficit, the partial correlation $r_{freq,SWP \cdot VPD}$ quantifies how much frequency and soil potential remain associated once the shared atmospheric cycle is removed, and so distinguishes a direct link from one that is only the by-product of the common daily forcing.

The two experimental groups, the water-stressed plants and the irrigated controls, were compared with the Mann-Whitney U test, a non-parametric test of whether one group tends to take consistently higher values than the other. The observations of the two groups are pooled and ranked together, and the rank sums form the statistic

$$U_1 = R_1 - \frac{n_1(n_1 + 1)}{2} \tag{3.7}$$

with R_1 the rank sum of the first group and n_1 its size, U_2 defined in the same way, and $U = \min(U_1, U_2)$. The test was applied to the per-plant coefficients, taking one plant as a single observation, because the sub-daily samples of one plant are strongly autocorrelated and cannot be treated as independent, whereas distinct plants can. In the water balance, the same Spearman coefficient is used to compare the stem frequency with the simulated crop evapotranspiration (Section 4.3).

3.3 Water balance

The daily water status of the root zone was reconstructed by coupling the measured soil water potential with a water balance of the substrate. The measured potential was first converted into volumetric water content through the substrate retention curve (Section 3.3.1). The reference evapotranspiration, which represents the atmospheric demand driving the water loss, was

computed from the greenhouse microclimate (Section 3.3.2) and used, together with a crop coefficient, to drive the AgrHyd model that tracks the depletion of the reservoir (Section 3.3.3). The balance was run on the subset of plants selected as described in Section 3.3.4. The simulated water content was then compared with the content derived from the measurements, so that the model could be assessed over each drying cycle.

3.3.1 From soil water potential to water content

The substrate used in the experiment is a commercial peat-based growing medium. Its physical properties were taken from the manufacturer technical datasheet (TS-3), which reports them following the EN 13041 standard for the determination of the physical properties of soil improvers and growing media. The properties relevant to the water balance are collected in Table 3.2.

The substrate water status was monitored as soil water potential (SWP), recorded by the instrument in kPa. The water balance operates on the amount of water stored in the root zone, so the potential was converted into volumetric water content through the water retention curve of the substrate, which gives the content held at each matric potential and is a property of the porous medium (Raviv et al., 2019). Potentials were expressed on the pF scale, defined as the base-ten logarithm of the equivalent water column,

$$pF = log_{10}(|SWP| \cdot 10.2) \tag{3.8}$$

with SWP in kPa and 10.2 the conversion from kPa to centimetres of water.

Four points of the retention curve were derived from the datasheet, listed in Table 3.3. Saturation was set equal to the total porosity of the substrate, $\theta_s = 0.90$ at pF 0. Field capacity, that is the water retained after free gravitational drainage, was taken at the -1 kPa pressure head (pF 1) at which EN 13041 fixes the drainage equilibrium for growing media, giving $\theta_{FC} = 0.62$ from the water volume reported at pF 1 (Londra et al., 2018; Raviv et al., 2019). The remaining two points were obtained by subtracting from the field capacity the available water fractions reported on the datasheet at the corresponding EN 13041 pressure heads, which gives $\theta = 0.37$ at pF 1.7 (-5 kPa) and $\theta = 0.33$ at pF 2 (-10 kPa). These four points span the functional range of the substrate, from full saturation to the dry condition.

The retention curve was described with the van Genuchten (1980) model,

$$\theta(h) = \theta_r + \frac{\theta_s - \theta_r}{[1 + (\alpha|h|)^n]^m}, \quad m = 1 - 1/n \tag{3.9}$$

with |h| the pressure head in centimetres. The four points were fitted by non-linear least squares, holding θ_s at the total porosity and leaving θ_r, α and n free. The fitted parameters are reported in Table 3.4. The model reproduced the four input points with a root mean square error of 0.003 $m^3\ m^{-3}$ (Table 3.5), and the resulting curve is shown in Figure 3.1.

The water balance requires two reference contents, read from the fitted curve: field capacity, $\theta_{FC} = 0.62$, is the upper limit of the water the substrate holds against gravity, and the wilting point, evaluated at -1500 kPa, the conventional limit of extraction by the crop; on the fitted curve this content coincides with the residual water content of the model, so $\theta_{WP} = \theta_r = 0.299$. These two values delimit the total available water that the model depletes (Section 3.3.3).

Table 3.2. Physical properties of the substrate from the technical datasheet (TS-3), reported per EN 13041.

Property	Value	Unit
pH (H_2O)	6.0	-
Electrical conductivity	0.56	dS m^{-1}
Dry bulk density	150	kg m^{-3}
Total porosity	90	% v/v
Air volume at pF 1	28	% v/v
Water volume at pF 1	62	% v/v
Easily available water	25	% v/v
Total available water	29	% v/v
Organic matter	78	%

Table 3.3. Retention points derived from the datasheet and used to fit the van Genuchten curve.

Point	Pressure head	pF	θ (m^3 m^{-3})	Source
Saturation	≈ 0	0	0.90	total porosity
Field capacity	-1 kPa (-10 cm)	1.0	0.62	water volume at pF 1
Intermediate	-5 kPa (-50 cm)	1.7	0.37	FC - easily available water (25%)
Dry point	-10 kPa (-100 cm)	2.0	0.33	FC - total available water (29%)

Table 3.4. Fitted van Genuchten parameters (θ_s held fixed at the total porosity).

Parameter	Value	Unit
θ_s (fixed)	0.900	m^3 m^{-3}
θ_r	0.299	m^3 m^{-3}
α	0.151	cm^{-1}
n	2.07	-
m = 1 - 1/n	0.517	-
RMSE of fit	0.003	m^3 m^{-3}

Table 3.5. Validation of the fit at the four datasheet points.

pF	θ observed	θ predicted	Residual
0	0.900	0.894	+0.006
1.0	0.620	0.621	-0.001
1.7	0.370	0.367	+0.002
2.0	0.330	0.332	-0.002

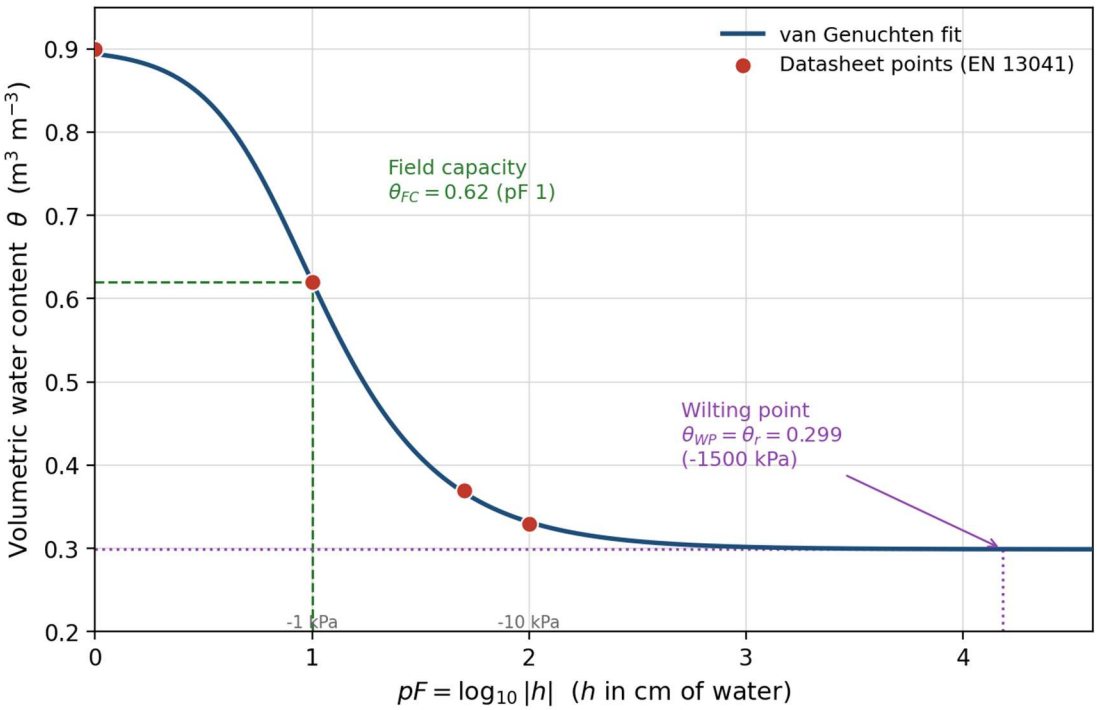


Figure 3.1. Water retention curve of the substrate. The van Genuchten model was fitted to the four datasheet points (EN 13041). Dashed lines mark the field capacity at pF 1 and the wilting point at -1500 kPa.

3.3.2 Reference evapotranspiration

The atmospheric water demand that drives the balance was described by the reference evapotranspiration ET_0, computed on a daily step with the FAO-56 Penman-Monteith equation (Allen et al., 1998),

$$ET_0 = \frac{0.408 \cdot \Delta \cdot (R_n - G) + \gamma \cdot \frac{900}{T + 273} \cdot u_2 \cdot (e_s - e_a)}{\Delta + \gamma \cdot (1 + 0.34 \cdot u_2)} \quad (3.10)$$

where R_n is the net radiation, G the soil heat flux, T the mean air temperature, u_2 the wind speed at 2 m, (e_s - e_a) the vapour pressure deficit, Δ the slope of the saturation vapour pressure curve and γ the psychrometric constant. The equation is the standard FAO-56 form for the reference grass surface, in which the aerodynamic and surface resistances are already incorporated in the numerical coefficients: the term 900/(T+273) and the factor (1 + 0.34·u2) at the denominator follow from the aerodynamic resistance ra = 208/u2 and the fixed surface resistance of the reference crop. The adaptation to the greenhouse therefore acts through the following inputs: the incoming radiation is attenuated by the cover, and a low internal wind speed is adopted, while the air temperature and relative humidity are those measured inside the greenhouse.

The net radiation was reconstructed from the incoming solar radiation. The outside solar radiation $R_{s,out}$ was measured by the regional ARPA station, and the fraction entering the greenhouse was obtained by applying a cover transmissivity $\tau = 0.70$, representative of the tempered glass covering of the Venlo-type structure (Baille, 1999),

$$R_{s,in} = \tau \cdot R_{s,out} \quad (3.11)$$

The net shortwave radiation followed as $R_{ns} = (1 - \alpha) \cdot R_{s,in}$, with a canopy albedo $\alpha = 0.23$ (Allen et al., 1998). The net longwave radiation R_{nl} was computed with the FAO-56 formulation from the internal maximum and minimum temperatures and the actual vapour pressure, using the clear-sky radiation derived from the extraterrestrial radiation R_a, itself a function of the site latitude ($\varphi = 45.06°$ N) and of the Julian day (Allen et al., 1998, Eqs. 21 to 25). The net radiation was then $R_n = R_{ns} - R_{nl}$. The soil heat flux was taken as negligible at the daily step, $G \approx 0$.

Since the wind speed inside the greenhouse was not measured, a value $u_2 = 0.3$ m s^{-1} was adopted, representative of the low air movement of a passively ventilated greenhouse, in line with the values used for unheated Mediterranean greenhouses (Orgaz et al., 2005). The choice is conservative for the poorly ventilated structure examined here, whose frequently high internal diurnal temperature range indicates limited air exchange, and its influence on the result is small, as the sensitivity analysis reported below shows. The wind speed enters the equation through the coefficient $(1 + 0.34 \cdot u_2)$, which embodies the aerodynamic resistance $r_a = 208/u_2$ of the reference surface (Allen et al., 1998); at the adopted $u_2 = 0.3$ m s^{-1} this corresponds to $r_a \approx 693$ s m^{-1}.

The saturation vapour pressure was computed as the mean of the values at the maximum and minimum daily temperatures, $e_s = [e°(T_{max}) + e°(T_{min})] / 2$, and the actual vapour pressure as $e_a = e_s \cdot RH_{mean} / 100$, from the internal relative humidity. The slope Δ and the psychrometric constant γ were obtained from the standard FAO-56 relations.

The resulting daily ET_0 series was supplied to the water balance model as an external forcing (Section 3.3.3). Over the July to September period of the plants used in the balance, ET_0 ranged between about 0.6 and 4.5 mm d^{-1}, with a period mean of 2.9 mm d^{-1} (Figure 3.2), in agreement with the daily values reported for unheated Mediterranean greenhouses (Fernández et al., 2010) and followed a decreasing seasonal trend consistent with the reduction of incoming radiation and mean temperature.

Table 3.6. Parameters adopted in the greenhouse FAO-56 Penman-Monteith computation of ET_0.

Parameter	Symbol	Value	Source
Cover transmissivity	τ	0.70	Baille, 1999
Canopy albedo	α	0.23	Allen et al., 1998
Wind speed at 2 m	u_2	0.3 m s^{-1}	Orgaz et al., 2005
Soil heat flux (daily)	G	≈ 0	Allen et al., 1998
Site latitude	φ	45.06° N	site (Grugliasco, TO)
Site elevation	z	293 m	site (Grugliasco, TO)
Solar constant	G_{sc}	0.082 MJ m^{-2} min^{-1}	Allen et al., 1998
Latent heat of vaporization	λ	2.45 MJ kg^{-1}	Allen et al., 1998

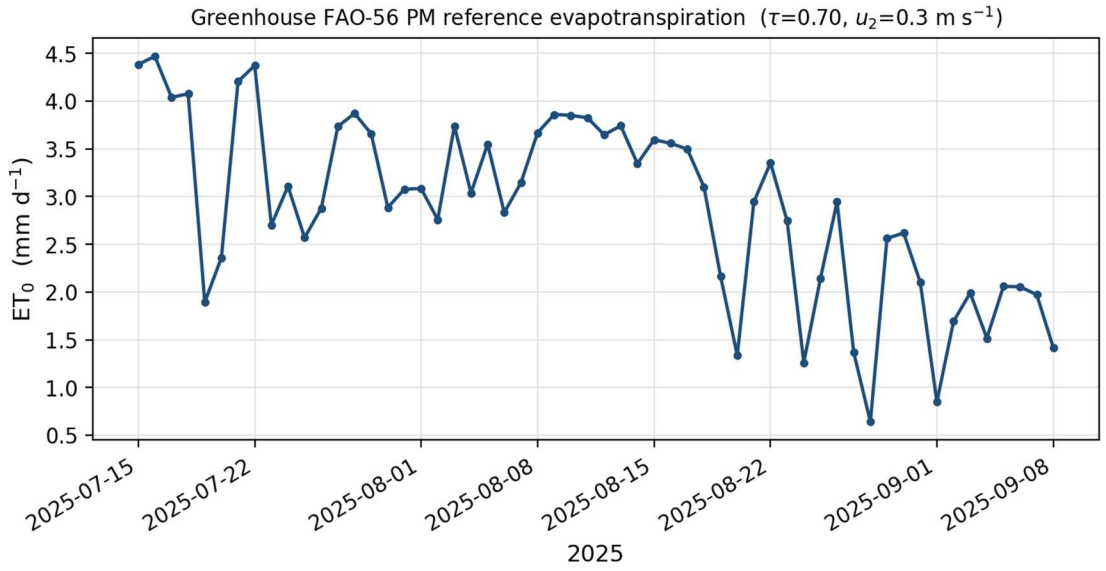


Figure 3.2. Daily reference evapotranspiration computed with the greenhouse FAO-56 Penman-Monteith equation ($\tau = 0.70$, $u_2 = 0.3$ m s^{-1}) over the July to September 2025 period.

To verify the Penman-Monteith estimates, the reference evapotranspiration was also computed with the temperature-based Hargreaves-Samani equation (Hargreaves and Samani, 1985; Allen et al., 1998),

$$ET_0 = 0.0023 \cdot R_a \cdot (T_{mean} + 17.8) \cdot (T_{max} - T_{min})^{0.5} \quad (3.12)$$

with R_a the extraterrestrial radiation expressed in equivalent evaporation units, and the greenhouse value obtained by applying the same cover transmissivity, $ET_{0,gh} = \tau \cdot ET_0$. This equation needs only the air temperature and the extraterrestrial radiation, so it provides an independent estimate that does not depend on the radiation and vapour pressure terms of the Penman-Monteith equation. The Hargreaves-Samani estimate ran systematically higher than the Penman-Monteith one, with a period mean of about 3.8 mm d^{-1} against 2.9 mm d^{-1}, and the difference widened on days with a large internal diurnal temperature range. This behaviour is expected, since the Hargreaves-Samani equation infers the evaporative demand from the temperature range alone and the confined environment amplifies that range through its limited air exchange, whereas the Penman-Monteith equation constrains the demand through the full energy balance and the vapour pressure deficit. The Penman-Monteith series was therefore retained as the reference input to the water balance, and the Hargreaves-Samani estimate was used only as a consistency check.

Because the two greenhouse-specific parameters, the cover transmissivity τ and the internal wind speed u_2, were assigned from the literature rather than measured, their influence on the reference evapotranspiration was examined over the whole study period. Figure 3.3 shows the period-mean ET_0 as a function of u_2 for a range of transmissivity values. The reference evapotranspiration responds almost linearly to the transmissivity, which scales the incoming radiation and hence the dominant radiative term, while its dependence on the wind speed is weak, since the aerodynamic term is small under the humid and poorly ventilated greenhouse air. Across the plausible ranges of the two parameters, τ from 0.60 to 0.80 and u_2 from 0.1 to 0.7 m s^{-1}, the transmissivity accounts for about 1 mm d^{-1} of variation in the period-mean ET_0, whereas the wind speed accounts for only about 0.4 mm d^{-1}. The adopted combination, $\tau = 0.70$ and $u_2 = 0.3$ m s^{-1}, gives a period-mean ET_0 of 2.89 mm d^{-1}, and the estimate is therefore robust

to the residual uncertainty on the wind speed, being controlled mainly by the transmissivity fixed from the optical properties of the glass cover.

The magnitude of these effects can be quantified over the study period (Table 3.7). Holding the wind speed at the adopted value, an increase of the transmissivity from 0.60 to 0.80 raises the period-mean ET_0 from 2.40 to 3.38 mm d^{-1}, a change of 0.98 mm d^{-1}, or about 34% of the adopted estimate, so that each step of 0.05 in τ shifts ET_0 by roughly 0.25 mm d^{-1}. Holding the transmissivity at 0.70, an increase of the wind speed from 0.1 to 0.7 m s^{-1} raises the period-mean ET_0 from 2.75 to 3.16 mm d^{-1}, a change of only 0.41 mm d^{-1}, or about 14%. Expressed as relative sensitivities around the adopted point, a 1% change in the transmissivity changes ET_0 by about 1.2%, whereas a 1% change in the wind speed changes it by about 0.07%. The reference evapotranspiration is therefore almost proportional to the transmissivity and nearly insensitive to the wind speed, which means that the internal wind speed has the smallest effect, while the cover transmissivity is constrained by the optical properties of the glass cover.

Table 3.7. Period-mean ET_0 (mm d^{-1}) for combinations of cover transmissivity τ and wind speed u_2, July to September 2025. The adopted combination is in bold.

τ \ u_2 (m s^{-1})	**0.1**	**0.3**	**0.5**	**0.7**
0.60	2.25	2.40	2.54	2.68
0.65	2.50	2.64	2.78	2.92
0.70	2.75	**2.89**	3.03	3.16
0.75	3.00	3.13	3.27	3.40
0.80	3.25	3.38	3.51	3.64

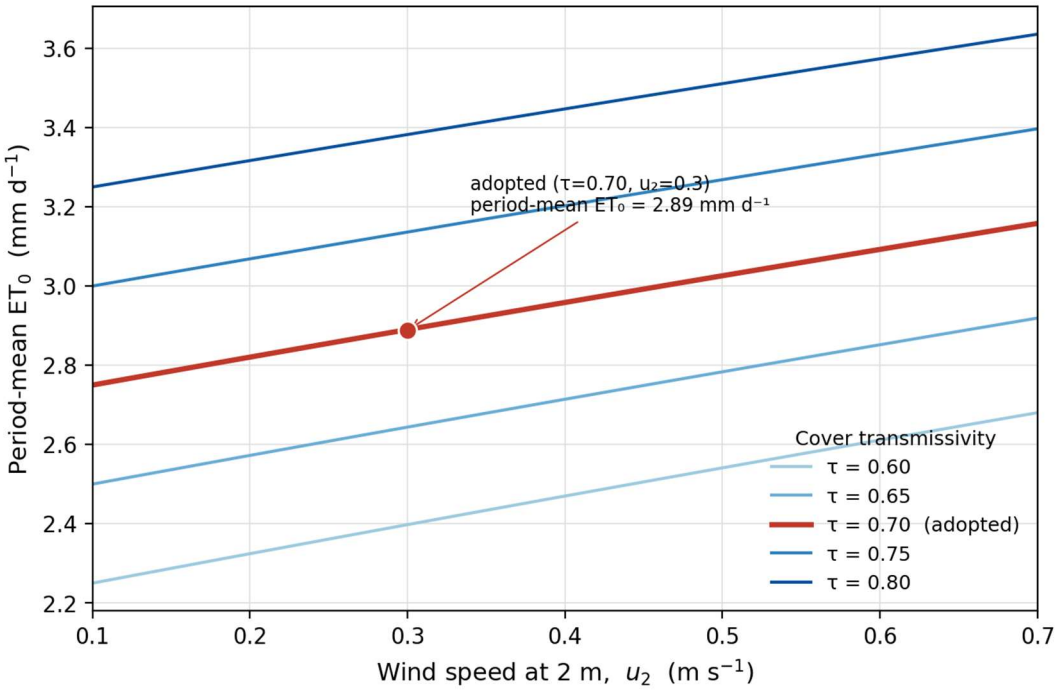


Figure 3.3. Sensitivity of the period-mean reference evapotranspiration to the cover transmissivity τ and the internal wind speed u_2, over the July to September 2025 period. The marked point is the adopted combination (τ = 0.70, u_2 = 0.3 m s^{-1}).

3.3.3 The AgrHyd water balance model

The water balance of the root zone was simulated with AgrHyd (Rolle et al., 2021), a model that follows the depletion of the soil water reservoir on a daily time step according to the FAO-56 procedure. The model was applied in its single-point configuration, forced with the climatic series measured in the greenhouse and with the retention properties of the substrate described in Section 3.3.1.

The state variable of the balance is the depletion Dr, the amount of water missing from the root zone with respect to field capacity, expressed as an equivalent depth of water:

$$D_r = (\theta_{fc} - \theta) \cdot Z_r \tag{3.13}$$

The reservoir is bounded by the total available water, the amount that separates field capacity from the wilting point:

$$TAW = (\theta_{fc} - \theta_{wp}) \cdot Z_r \tag{3.14}$$

With the retention parameters of the substrate and a rooting depth of 0.14 m, TAW amounts to 44.9 mm. The threshold beyond which the crop can no longer extract water at the potential rate is a fixed fraction of this reservoir, the readily available water:

$$RAW = p \cdot TAW \tag{3.15}$$

where p is the depletion factor, kept at the value tabulated for tomato (p = 0.40), giving RAW = 18.0 mm.

At each daily step the model evaluates the water stress coefficient from the depletion reached at the end of the previous day,

$$K_s = \frac{TAW - D_r}{TAW - RAW} \tag{3.16}$$

bounded to the interval [0, 1], so that Ks equals unity while the depletion remains below RAW and decreases linearly to zero as the reservoir is emptied. The evapotranspiration of the day is then with equation 2.1, and the depletion is updated by adding it to the value of the previous day, the inputs being zero for the non-irrigated plants under cover:

$$D_r(t) = D_r(t - 1) + ET_c(t) \tag{3.17}$$

The depletion is constrained to the interval between zero and TAW, so that the water content of the root zone cannot exceed field capacity nor fall below the wilting point. The model returns the available water content of the root zone, $WCrz = \theta - \theta_{wp}$, from which the simulated volumetric water content is recovered as $\theta_{sim} = WCrz + \theta_{wp}$.

Two features of this formulation are relevant to the interpretation of the results. First, water more than field capacity is not carried by the balance: the depletion is bounded below at zero, so that a water content prescribed above field capacity is reduced to it at the first step, and the excess is not accounted for as drainage. The model thus represents a substrate that has already lost its gravitational water, and the drainage term is inactive for a closed pot under cover. Second, the stress coefficient remains at unity over the first part of the drying: with the values above, the depletion reaches RAW only after about five days at the evapotranspiration rates observed in summer, so that over the initial part of the comparison interval the model evaporates at its maximum rate, unreduced by stress.

The rooting depth was set equal to the depth of the container (Zr = 0.14 m) and kept constant. In the FAO-56 procedure the rooting depth increases through the season as the roots explore a deeper profile, but this does not apply to cultivation in a container of limited depth, where the volume available to the plant is fixed by the geometry of the pot and is assumed to be fully explored at the beginning of the monitoring, the plants having been transplanted as developed seedlings.

Among the parameters read by the model, the critical water content is loaded but does not enter the water balance in the single crop coefficient formulation, and it was verified that varying it leaves the simulated series unchanged.

3.3.4 Plant selection and comparison

The water balance was applied to a subset of the monitored plants, chosen to meet the requirements of the model. Three criteria guided the selection.

First, only plants under the abiotic-stress treatment were considered. The irrigated controls do not undergo a drying cycle, so their root-zone storage stays close to field capacity and offers no depletion to reproduce, while the biotic-stress plants cannot be represented by a water balance.

Second, the balance uses the absolute value of the soil water potential, since this is converted into water content through the retention curve (Section 3.3.1). The Watermark sensor returns reliable values only within its range, from 0 to about -239 kPa (Section 3.2), so only plants and periods whose potential stays within, or remains usefully ordered close to, this range were retained. This set aside the clusters in which the sensor saturated over most of the record, and the plants in which a genuine drying never developed, such as those of cluster C4, whose potential never fell below about -32 kPa.

Third, the reference evapotranspiration that forces the balance must be well defined. The warm-season clusters give a positive and physically consistent ET_0 over the whole period, whereas the late-autumn cluster produced spells of near-zero or negative ET_0 under the low winter radiation of the site (Section 3.3.2), which fall outside the validity of the FAO-56 framework. The warm-season clusters were therefore preferred.

Applying these criteria left two clusters, C2 (May to July 2024) and C7 (July to September 2025), each providing four abiotic-stress plants with a usable soil water potential. The eight selected plants are listed in Table 3.8. Together they span a wide range of initial water content, from values close to field capacity to values already close to the wilting point, so that the model could be tested both on plants that dry out from a nearly full substrate and on plants that are already dry at the beginning of monitoring.

Table 3.8. Plants selected for the water balance.

Plant	Cluster	Period	Duration (days)	θ at day 1 (m^3 m^{-3})
P16	C2	May-Jul 2024	38	0.712
P17	C2	May-Jul 2024	38	0.363
P18	C2	May-Jul 2024	38	0.750
P19	C2	May-Jul 2024	38	0.749
P79	C7	Jul-Sep 2025	56	0.382

Plant	Cluster	Period	Duration (days)	θ at day 1 (m^3 m^{-3})
P80	C7	Jul-Sep 2025	56	0.765
P81	C7	Jul-Sep 2025	56	0.392
P82	C7	Jul-Sep 2025	56	0.345

Chapter 4 Results

4.1 Dataset overview and behavioural classes

The analyses in this chapter are based on the stem-frequency measurements collected from the tomato plants over the seven clusters monitored between 2024 and 2025. Each cluster comprised plants kept under regular irrigation and plants subjected to progressive water deprivation, so that a stressed group was always monitored alongside an irrigated control. The plants exposed to biotic stress, followed within the same project, lie outside the scope of this work. Besides the stem frequency, each plant carried a Watermark soil water potential sensor and temperature and relative humidity probes, sampled every 10 or 20 minutes, while the incoming radiation was taken from the nearest ARPA station at daily resolution. The condition, period and cluster of each plant are summarised in Table 4.1.

The series were screened for artefactual spikes in the frequency and for the validity of the soil water potential following the procedure of Section 3.2. For most plants the flagged fraction of the frequency was negligible, below about one per cent, and the series was used as it stood; for a few plants it reached about eleven per cent, concentrated in the first days of monitoring, before the sensor connection had stabilised, and for these the initial portion of the record was discarded. After this screening, three plants (P33, P75 and P77) were excluded for the lack of usable frequency data, one plant (P68) for not surviving its cluster, and one record (P83) for duplicating that of another plant (P76). Two irrigated plants (P38 and P47) were retained but flagged, since their soil water potential stayed pinned at the sensor full-scale value, about -1233 kPa, while their frequency followed the pattern of the irrigated plants, which points to a Watermark fault rather than to real water stress.

The reliability of the soil water potential varies markedly between clusters, since the Watermark sensor loses accuracy beyond -239 kPa (Section 3.2). The last column of Table 4.1 reports, for each cluster, the fraction of the stressed-plant records that falls beyond this limit. It ranges from clusters that stay entirely within the valid range, such as C1 and C4, to the late-autumn cluster C5, where most of the record lies beyond it. This fraction, together with the length of the cluster and the season, guides the use that each cluster can support, and in particular the selection of the clusters used for the water balance (Section 3.3.4).

Table 4.1. Clusters of the experiment: period, duration, plants by condition, and fraction of the stressed-plant soil water potential falling beyond the Watermark reliable range (-239 kPa).

Cluster	Period	Duration (days)	Irrigated	Abiotic stress	SWP beyond -239 kPa
C1	Mar-Apr 2024	10	P0-P3	P4-P7	0%
C2	May-Jul 2024	38	P11-P15	P16-P19	3-16%
C3	Jul-Sep 2024	44	P25-P29	P30	≈52%
C4	Sep-Oct 2024	31	P34-P38	P39-P42	0%
C5	Oct-Dec 2024	54	P47-P51	P52-P55	60-73%
C6	Apr-May 2025	46	P61-P65	P66, P67, P69	31-41%

Cluster	Period	Duration (days)	Irrigated	Abiotic stress	SWP beyond -239 kPa
C7	Jul-Sep 2025	56	P76, P78	P79-P82	40-52%

4.2 Stem-frequency analysis

This section presents the results of the stem-frequency analysis in two parts: the qualitative behaviour of the signal and its correlation with the water and atmospheric variables (Section 4.2.1), and the functional form and the timing of its relationship with the soil water potential (Section 4.2.2).

4.2.1 Behaviour and correlation of the stem frequency

The temporal behaviour of the stem frequency is first described in the two groups, cluster by cluster. Cluster C1 is not considered, for two reasons: the monitoring lasted only ten days, too short for a stress condition to develop, and its stressed and irrigated plants are poorly matched in their initial water content. In cluster C2 the frequency of the stressed plants follows a trend like that of the irrigated ones, although a difference in the maximum and minimum values is still visible, with the stressed plants confined to a slightly lower range, and these values are consistent among plants in the same condition. In cluster C3 the stressed plant follows the irrigated ones closely until the soil begins to dry, at which point its frequency falls below its own initial level. Cluster C4 shows no appreciable difference between the two conditions, in agreement with a soil water potential that never reached values indicative of real stress. In cluster C5 (P47 excluded) the frequency of the stressed plant drops from the outset, its initial water content being already close to the wilting point (about 31 per cent), and the two conditions are clearly distinguishable. In cluster C6 (P65 and P68 excluded) the stressed plants fall once they enter severe stress, forming a final tail, while the irrigated ones return to a minimum comparable to their starting value. Cluster C7 behaves like C5 and C6, with a clear divergence between the two conditions. Figure 4.1 shows an example of behaviour of different plants in different condition, for one cluster.

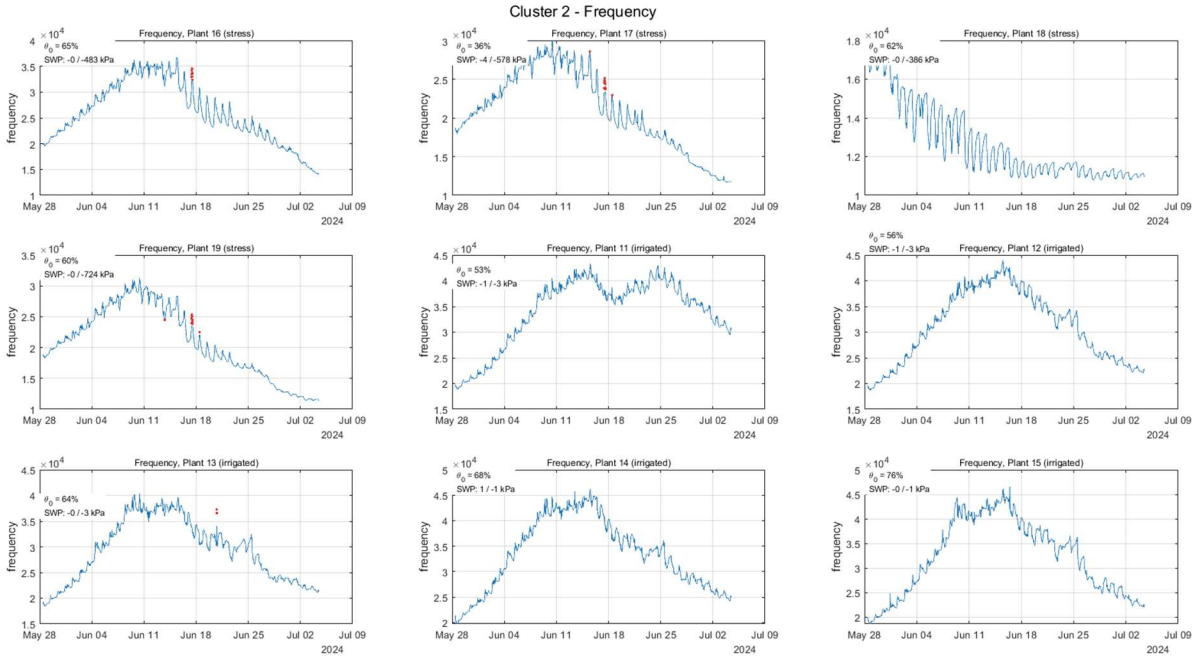


Figure 4.1. stem frequency, stressed vs irrigated plants, cluster C2.

Within each cluster, a stressed plant and an irrigated one with similar initial soil moisture (θ_0) are compared directly, to see whether the two frequencies follow a comparable trajectory in the early phase and then separate, as expected if the frequency tracks water stress. The behaviour differs across clusters (figure 4.2). In cluster C2 the two plants have nearly identical initial moisture (65 and 64 per cent): both curves rise together until mid June and reach the plateau at a similar level, after which the stressed plant declines while the irrigated one remains high, so the trajectory is a shared growth phase followed by a downward segment present only in the stressed plant. Cluster C6 shows an analogous pattern, with the irrigated plant slightly higher during growth. In cluster C4 the two curves stay close for the whole period and separate only marginally at the end, consistent with a potential that reached only -15 to -32 kPa: the absence of stress corresponds to the absence of separation. In cluster C3 the stressed plant rises above the irrigated one, reaches a higher peak and then falls below it, a phase of growth followed by decline. In clusters C5 and C7 the stressed plant shows no growth phase: it stays low, or declines early, while the irrigated plant rises, so the separation is present from the start. The matching on θ_0 is close in clusters C2, C5 and C6 but not in C1 (31 against 93 per cent) and C7 (53 against 76 per cent), where part of the difference may reflect the initial moisture rather than the treatment; for this reason C7 is kept only as a graphical example and the argument rests on the matched pairs C2, C5 and C6.

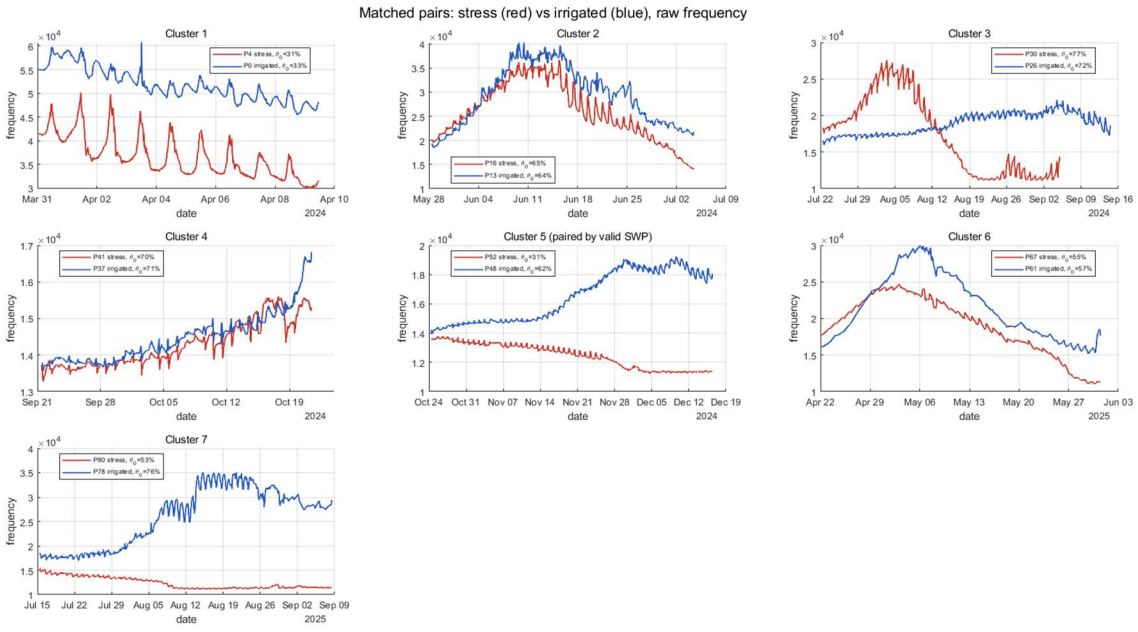
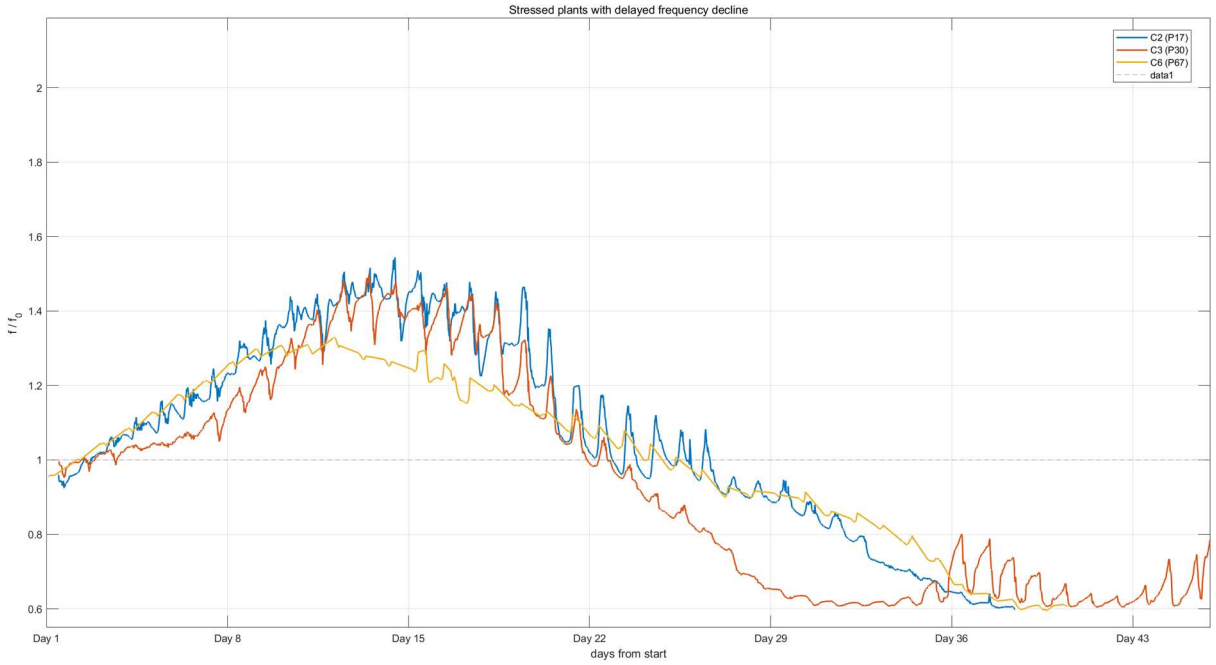


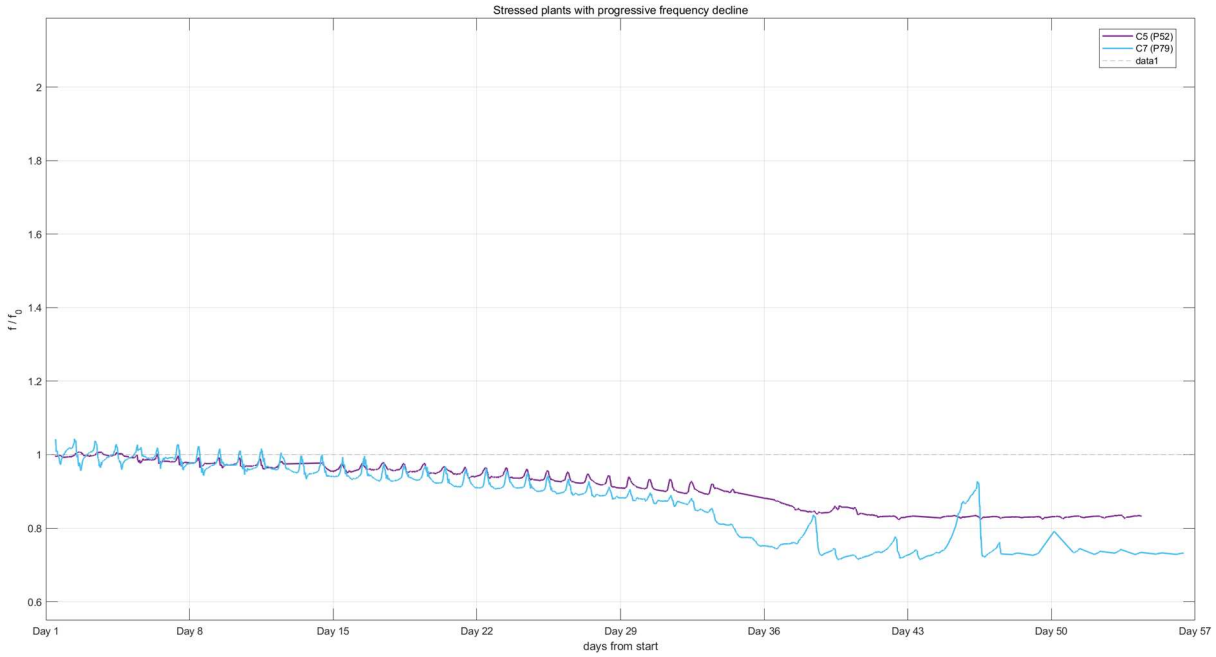
Figure 4.2. Matched-pair comparison (θ_0-matched stressed vs irrigated), for each cluster.

The plants were then grouped according to the observed trajectory of the stem frequency, given that the nominal condition does not always correspond to the actual behaviour of the signal: the development of water stress depended on the conditions effectively reached in each cluster. Five behavioural classes were identified (Table 4.2), and plotted separately (Figure 4.3). Among the abiotic-stress plants three patterns emerge: a first class in which stress never actually developed, the frequency following a growth-driven trajectory with no dehydration phase; a second in which the frequency follows the irrigated controls, a shared growth phase and plateau diverging only in a final decline; and a third in which the frequency declines progressively, the stress response dominating. The irrigated controls split into two further classes according to whether the frequency, after the initial growth, keeps increasing or settles onto a plateau. Each class recurs across plants from different clusters, which supports reading these patterns as a property of the signal rather than an artefact of a single cluster.

Table 4.2. Classification of the monitored plants into five behavioural classes based on the observed stem-frequency trajectory. The first class was not representative of the nominal treatment under which it was classified.

Behavioural class	**Treatment**	**Clusters**	**Plants**
Stressed, no developed stress	Abiotic	C4	P39-P42
Stressed, delayed decline	Abiotic	C2, C3, C6	P16-P19; P30; P66, P67, P69
Stressed, progressive decline	Abiotic	C5, C7	P52-P55; P79-P82
Irrigated, monotonic increase	Irrigated	C4, C5	P35-P38; P51
Irrigated, growth-plateau	Irrigated	C2, C3, C4, C5, C6	P11-P15; P25-P29; P34; P48-P50; P61-P65


Stressed plants with delayed frequency decline
C2 (P17)
C3 (P30)
C6 (P67)
data1
f / f0
2
1.8
1.6
1.4
1.2
1
0.8
0.6
Day 1
Day 8
Day 15
Day 22
Day 29
Day 36
Day 43
days from start


Stressed plants with progressive frequency decline
C5 (P52)
C7 (P79)
data1
f / f0
2
1.8
1.6
1.4
1.2
1
0.8
0.6
Day 1
Day 8
Day 15
Day 22
Day 29
Day 36
Day 43
Day 50
Day 57
days from start

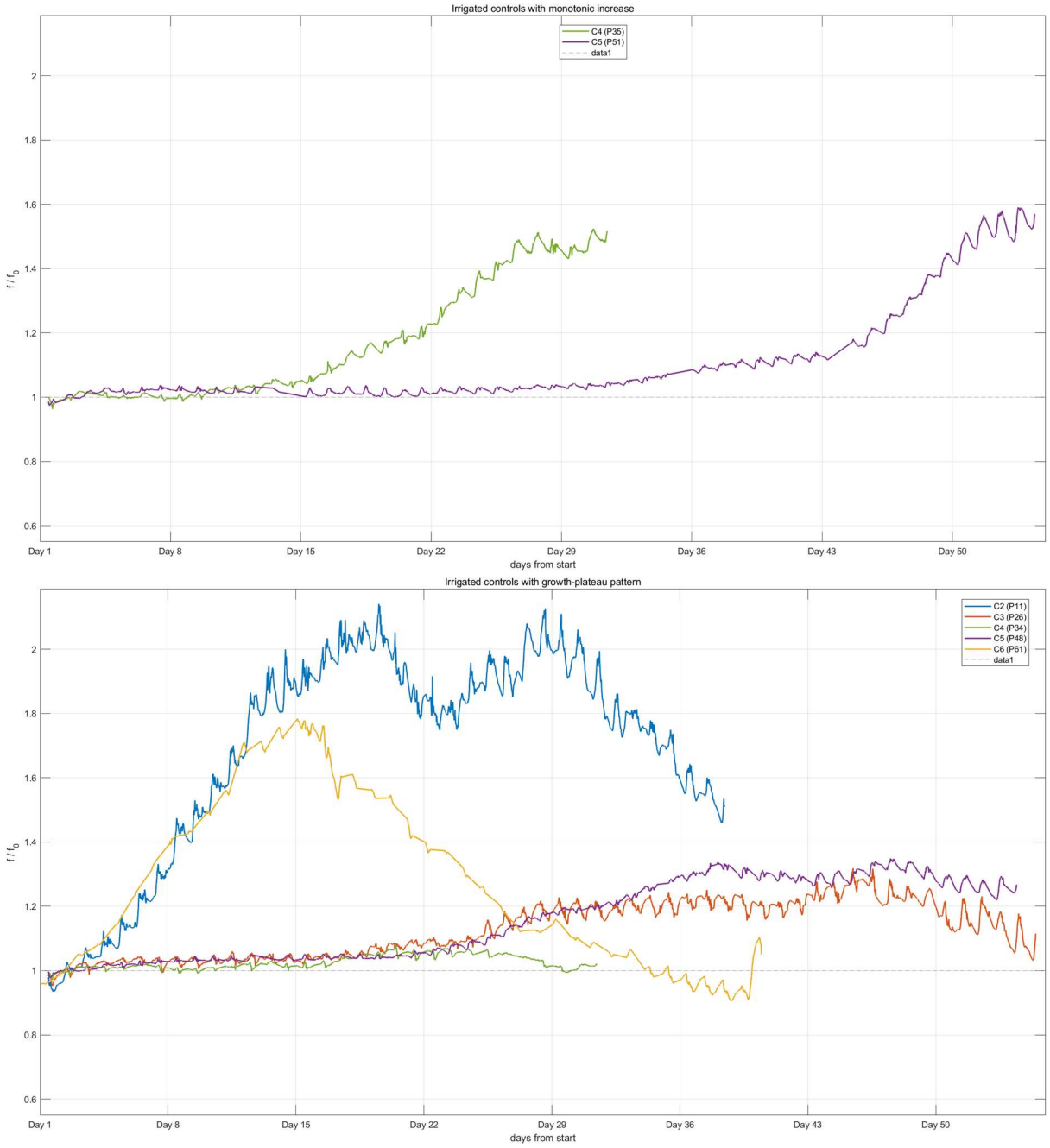


Figure 4.3. Representative stem-frequency trajectories for the behavioural classes, one representative plant per cluster within each class.

This qualitative separation is confirmed quantitatively by correlation analysis. The frequency was correlated against two variables sampled at the same sub-daily resolution: the soil water potential (SWP), representing the water available at the roots, and the vapour pressure deficit (VPD), representing the evaporative demand of the atmosphere. The stressed plants and the irrigated controls were analysed separately, and, besides the simple coefficients, partial correlations were used to isolate the response of the frequency to soil water from its response to atmospheric demand; because the repeated samples of one plant are strongly autocorrelated, the two groups were compared at the level of the individual plant, taking each plant's coefficient as one observation and applying the Mann-Whitney test (Section 3.2).

In the stressed plants the frequency shows a strong positive correlation with the soil water potential, with a median Spearman coefficient of 0.87, whereas in the irrigated plants it is

effectively absent, with a median of -0.10; the difference is highly significant (Mann-Whitney, $p < 0.0001$). The result is unchanged, and if anything reinforced, once the vapour pressure deficit is partialled out: the median partial correlation is 0.91 in the stressed group against -0.04 in the irrigated one, again with $p < 0.0001$. The link between frequency and soil water is therefore not a by-product of the common diurnal cycle but holds independently of the atmospheric demand. The correlation with the vapour pressure deficit behaves differently: in its simple form it does not separate the two groups ($p = 0.29$), and only once the soil water potential is held constant does a weak but significant difference emerge, with a median partial freq-VPD of -0.25 in the stressed group against -0.04 in the irrigated one ($p = 0.006$). This residual is small relative to the freq-SWP contrast and is best read as a secondary effect. The stem frequency therefore tracks the soil water condition specifically in the plants undergoing water deprivation: the signal acquires diagnostic meaning under stress and remains uninformative in well-watered plants. The correlations are represented through a boxplot graph in figure 4.4, where the central mark indicates the median, and the bottom and top edges of the box indicate the 25th and 75th percentiles, respectively.

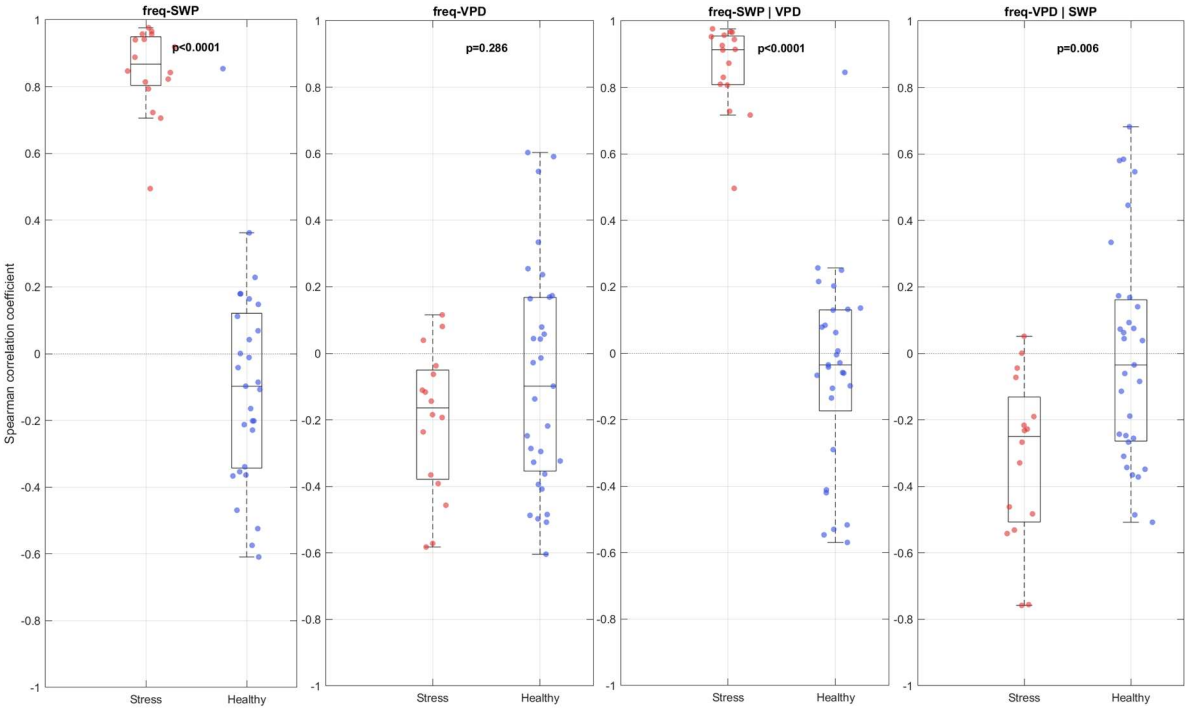


Figure 4.4. Per-plant partial correlations: freq-SWP (with VPD fixed) versus freq-VPD (with SWP fixed); stressed plants cluster at high freq-SWP, irrigated controls scatter around zero.

Two cases stand apart and reinforce the reading. In cluster C4 the four plants assigned to the stress treatment (P39 to P42) never developed a real deficit, their potential staying above about -32 kPa; their frequency keeps rising with growth and, correlated against a potential that barely moves, even returns negative coefficients, so they were excluded from the group comparison, confirming that the frequency follows the actual water status rather than the nominal treatment (the growth-driven rise is taken up in Section 5.1). In the opposite direction, a single irrigated plant, P48, behaves as if stressed, its frequency tracking the potential closely ($\rho = 0.85$), most plausibly because of an unrecorded dry spell; it is kept but flagged and does not affect the group separation.

The freq-SWP correlation is a stable feature of the signal rather than an effect of sub-daily noise. Repeating the analysis on smoothed series leaves it essentially unchanged: in the stressed group the median coefficient rises only marginally, from 0.87 on the raw data to 0.92 at the 24

h window, while the irrigated controls stay near zero and the separation remains highly significant at every level (Table 4.3). The freq-VPD correlation behaves in the opposite way: it does not separate the groups on the raw data, and at the 24 h window the coefficients of both groups drift towards negative values, the irrigated controls reaching -0.36. The link with soil water thus resides in the slow drying trend and survives the removal of the daily cycle, whereas the link with atmospheric demand resides in the circadian cycle and disappears once that cycle is averaged out, so the two relationships operate on different time scales, consistent with the timing analysis of Section 4.2.2.

Table 4.3. Median per-plant Spearman correlation of stem frequency with SWP and with VPD, on the raw signal and on signals smoothed with a moving average (6 h and 24 h windows), with the Mann-Whitney p-value between groups.

Correlation	Group	raw	6 h	24 h
Freq-SWP	Stressed (median)	0.87	0.88	0.92
	Irrigated (median)	-0.10	-0.09	-0.05
	Mann-Whitney p	<0.0001	<0.0001	<0.0001
Freq-VPD	Stressed (median)	-0.16	-0.17	-0.24
	Irrigated (median)	-0.10	-0.11	-0.36
	Mann-Whitney p	0.29	0.36	0.87

4.2.2 Form and timing of the frequency-SWP relationship

4.3 Water balance

The water balance was run on the eight selected plants (Section 3.3.4) with the AgrHyd model (Section 3.3.3), and the simulated water content was compared, day by day and over the whole monitoring series of each plant, with the content derived from the measured potential through the retention curve (Section 3.3.1). This section reports the outcome, both quantitative and qualitative (Figures 4.6 and 4.7); its interpretation is developed in Chapter 5.

The crop coefficient was determined on the two plants that begin at field capacity, one per cluster (P16 for C2, P80 for C7), by comparing constant and ramped forms across the FAO-56 range for tomato (Table 4.5). The two plants behave differently above the mid-season value: on P16 the error keeps decreasing as the coefficient is raised, reaching 0.037 at Kc = 1.30, so its minimum would lie outside the physically admissible range, whereas on P80 the constant 1.15 is already close to the minimum and higher values do not improve the fit. The value adopted is therefore not the one that minimises the error but the highest with physical meaning for tomato, the constant Kc = 1.15, the maximum tabulated by FAO-56 at full canopy. A staged form was also tested, with the development-to-plateau transition placed at the day on which the frequency of the irrigated plants stabilises (day 14 for C2, day 25 for C7) and the initial value read backwards from the FAO curve; it does not improve on the constant (RMSE 0.049 against 0.042 for P16) and imposes a phenological transition the data do not resolve, so the constant value is retained for parsimony.

Table 4.5. Crop coefficient determination: RMSE between simulated and observed water content over the whole series, for the two reference plants (θ_{wp} = 0.299, depletion factor 0.40).

K_c form	P16 RMSE	P80 RMSE
ramp 0.80 → 0.90	0.101	0.140
constant 1.00	0.053	0.116
ramp 1.00 → 1.15	0.073	0.116
ramp 0.97 → 1.15 + plateau	0.049	0.060
constant 1.15	0.042	0.039
constant 1.20	0.041	0.044
constant 1.30	0.037	0.040

With the constant coefficient the eight plants separate into two groups according to their water content at the start of monitoring (Table 4.6). The four plants that begin at field capacity are reproduced with a systematic positive bias, the simulated content lying above the observed one on every day, with RMSE between 0.039 and 0.057 and bias between +0.003 and +0.031. The four plants that begin already within the release range are reproduced closely, with RMSE markedly smaller, between 0.003 and 0.012, and a small negative bias. The separation follows the initial water content and not the cluster or the record length: the two groups each contain plants from both clusters, and P17, which has the longest usable record, falls in the low-error group. A few days on which the observed content rises, physically impossible in a non-irrigated plant and attributable to probe artefacts, were excluded from the metrics.

Table 4.6. Agreement between simulated and observed water content, ordered by decreasing initial water content.

Plant	Cluster	θ day 1	Initial condition	RMSE	Bias	MAE
P80	C7	0.765	field capacity	0.039	+0.007	0.016
P18	C2	0.750	field capacity	0.052	+0.026	0.038
P19	C2	0.749	field capacity	0.057	+0.031	0.042
P16	C2	0.712	field capacity	0.042	+0.003	0.026
P81	C7	0.392	observed	0.003	+0.000	0.002
P79	C7	0.382	observed	0.003	-0.000	0.002
P17	C2	0.363	observed	0.012	-0.008	0.008
P82	C7	0.345	observed	0.006	-0.003	0.004

The error of the field-capacity plants is concentrated in time rather than spread over the record. Decomposing the sum of squared errors of P16 shows that the first six days carry an RMSE of 0.074 and about 46 per cent of the total, while the remaining thirty days carry an RMSE of only 0.031 (Table 4.7). The same first-days error of about 0.074 persists for every crop coefficient

from 1.00 to 1.30, so the disagreement is not a matter of the amplitude that the coefficient controls but of the shape of the early drying.

Table 4.7. Time distribution of the error for P16: RMSE and share of the total sum of squared errors over increasing initial windows and over the remainder of the record.

Window	RMSE	n	Share of SSE
first 4 days	0.083	4	38%
first 6 days	0.074	6	46%
first 8 days	0.073	8	61%
remainder (from day 8)	0.031	30	39%

To locate the missing water, the daily decrease of the observed content was converted into an equivalent depth over the substrate and compared with the evapotranspiration simulated over the same days (Table 4.8). For the plants that begin at field capacity the observed loss exceeds the simulated evapotranspiration by a large factor, 1.75 for P16 and 2.67 for P80: on P80 the derived content implies that about 60 mm left the substrate in six days against 23 mm of evapotranspiration, a difference that no plausible evapotranspiration can cover. The ratio does not split the plants into two discrete regimes but decreases monotonically with the initial water content, from 2.67 in the wettest to about 1.45 in those beginning just below field capacity and to unity or below in the driest. The excess therefore scales with the amount of water held above field capacity at the start of monitoring; it cannot be accounted for by the evapotranspiration, and its interpretation is taken up in Section 5.2.

Table 4.8. Mass balance over the first days of drying: observed water loss against simulated evapotranspiration (equivalent depths of water).

Plant	θ day 1	n	Observed loss (mm)	Simulated ET (mm)	Ratio
P80	0.765	6	60.4	22.6	2.67
P16	0.712	9	40.3	23.0	1.75
P81	0.392	3	6.9	4.7	1.47
P79	0.382	3	6.1	4.2	1.45
P17	0.363	10	3.7	5.2	0.71
P82	0.345	2	1.6	1.7	0.93

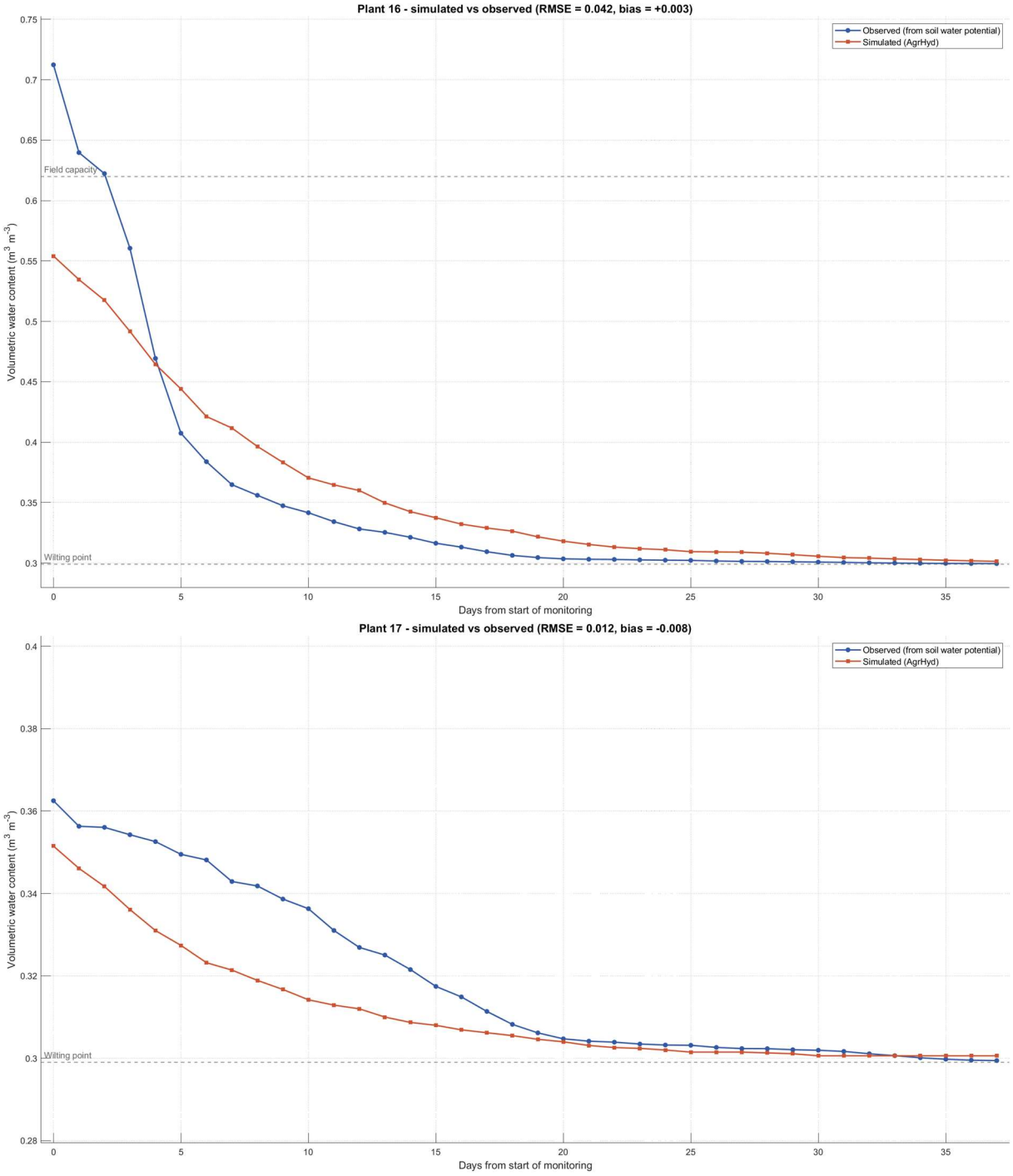


Figure 4.6. Simulated (red) and observed (blue) water content for P16 (starts at field capacity, model stays above) and P17 (starts dry, close agreement).

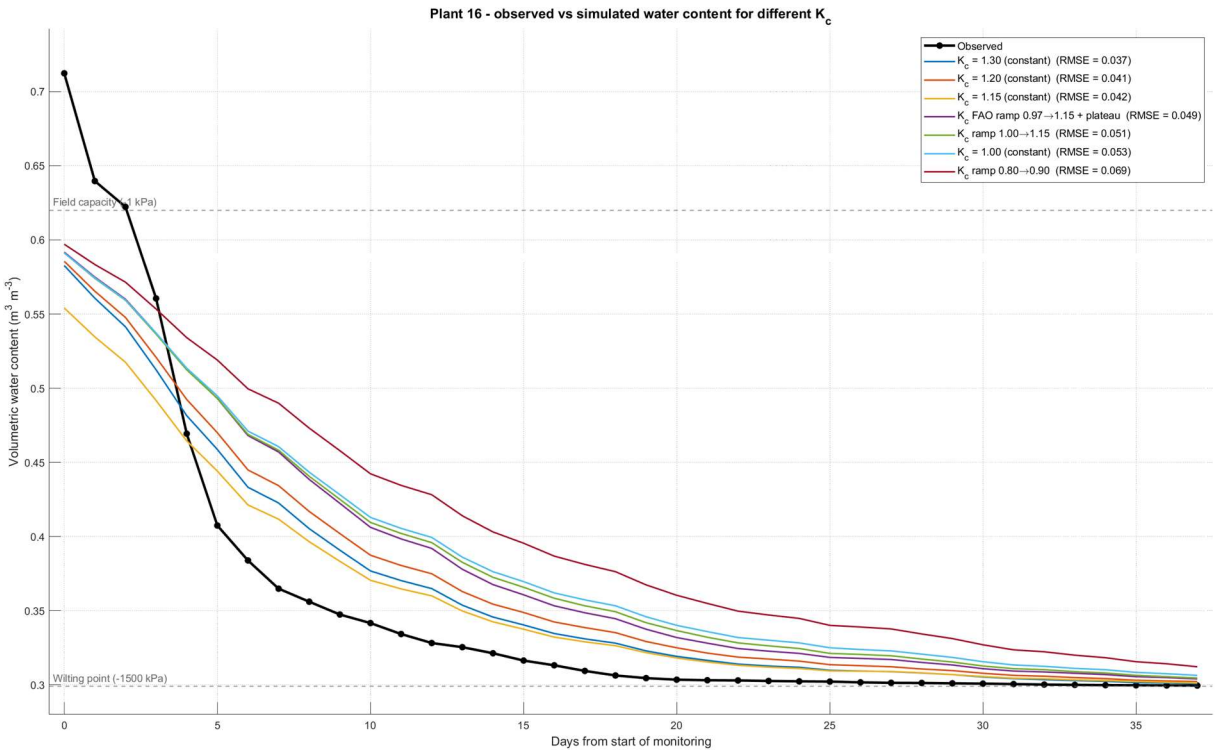


Figure 4.7. Observed water content of P16 against simulations with different crop coefficients; all lie above the observations in the steep part and converge on the same plateau.

Finally, the two approaches were brought together by comparing the stem frequency measured on the plant with the crop evapotranspiration simulated by the model (Figures 4.8 and 4.9). Both are daily series available for the same plants over the same period, so their association can be quantified directly with the Spearman rank coefficient (Table 4.9). The two are positively correlated in every plant, with coefficients between 0.73 and 0.96, but the extent of the record over which the association holds differs between the two clusters. In the C2 plants, which begin at field capacity and pass through a growth phase before drying, the correlation is modest over the whole record and becomes high only from the onset of the stress phase, taken at day 14 for P16 and day 12 for P17; for P16 the coefficient rises from 0.45 over the full series to 0.87 over the stress phase alone. In the C7 plants, which are already dry at the start of monitoring and therefore under deficit throughout, the coefficient is high over the entire record, from 0.73 for P80 to 0.96 for P81. The correlation is concentrated in the phase in which the water deficit governs the plant, and its interpretation is developed in Section 5.3.

Table 4.9. Spearman correlation between the daily mean stem frequency and the simulated crop evapotranspiration, for the stressed plants (stress phase for the C2 plants, whole series for the C7 plants).

Plant	Cluster	Spearman ρ	Interval used
P16	C2	0.87	stress phase (from day 14)
P17	C2	0.78	stress phase (from day 12)
P79	C7	0.91	whole series
P80	C7	0.73	whole series
P81	C7	0.96	whole series

Plant	Cluster	Spearman ρ	Interval used
P82	C7	0.92	whole series

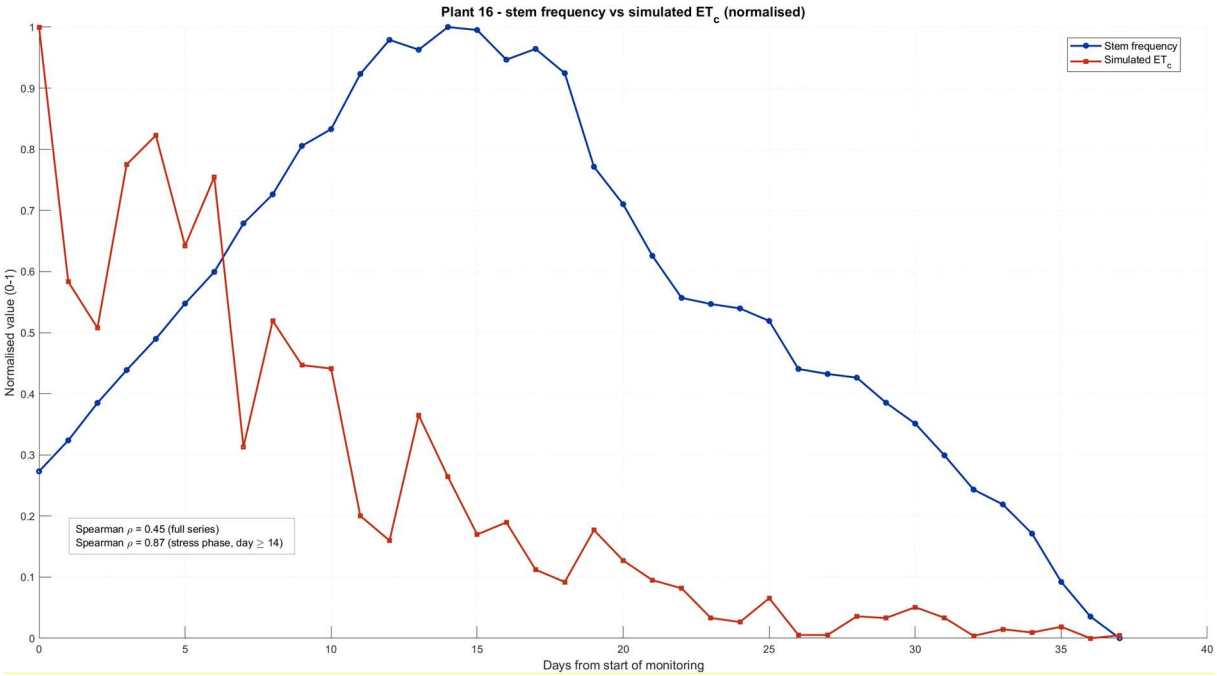


Figure 4.8. Normalised stem frequency and simulated ETc over time for P16 (C2): the two diverge during the growth phase and converge from the onset of stress.

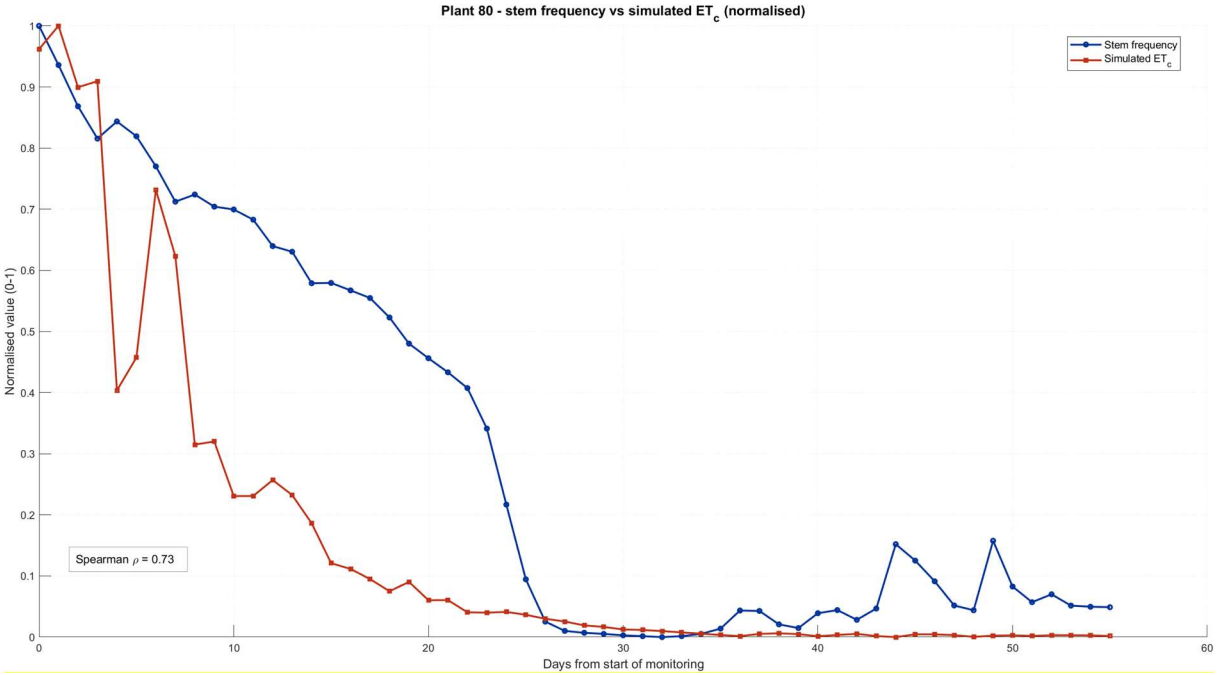


Figure 4.9. Normalised stem frequency and simulated ETc over time for P80 (C7): the two decline together over the whole record.

Chapter 5 Discussion

5.1 The stem frequency as a water-stress indicator

The central result of the frequency analysis is that the stem frequency responds to the soil water potential only in the plants that are drying. In the stressed plants the two are strongly correlated, with a median Spearman coefficient of 0.87, and the correlation survives, and even strengthens, once the atmospheric demand is removed, reaching a median partial coefficient of 0.91, whereas in the irrigated controls it is absent and the two groups are separated with a high level of significance. This selectivity is what makes the frequency a useful indicator of water stress: the signal carries information about the water condition of the plant precisely in the plants that are experiencing a deficit, and stays uninformative in those that are not, so that a change in the frequency can be read as a change in water status rather than as background variability. Formulated in these terms the result is a statement about when the signal becomes diagnostic, which is the form in which it is most useful for irrigation management.

This behaviour follows from what the frequency measures. The signal is set by the electrical impedance of the stem, which depends in turn on the water held in the tissue and on the ions dissolved in it (Chapter 2): as the tissue loses water its impedance rises, and the oscillator frequency falls accordingly. The direction of this response is well established in the literature and has been observed with a variety of electrode configurations and plant species. Garlando et al. (2022) report that the stem electrical impedance rises as the plant dries out and drops again after watering, the same inverse relationship on which the frequency signal used here rests. Comparini et al. (2020), working on olive with electrodes inserted in the stem, associate the electrical properties of the stem with the imposed water stress, and Zhang et al. (2024), measuring electrical impedance spectra on tomato stems, find impedance negatively correlated with water content. Serrano-Finetti et al. (2023) note that the absolute values reported by different studies differ by orders of magnitude, from the ohms of stem-inserted electrodes to the tens of kiloohms of surface electrodes on leaves, because the measurement protocols, the electrode geometry and the measurement site are largely ad hoc, yet all of them agree on the direction of the effect, an increase of impedance with decreasing water content. The present results sit within this consensus: they confirm the direction of the relationship in vivo and continuously, on intact potted plants, while inheriting the same limitation that the absolute values are specific to this measurement configuration and are not transferable as calibrated water contents.

In a plant under water deprivation the water status of the stem follows the declining soil potential, so the frequency tracks the soil water potential; in a well-watered plant the tissue stays hydrated and buffered against the daily fluctuations, so the frequency reflects the growth of the stem rather than its water status, which is why the controls show no correlation. This also explains the decline seen in some irrigated plants: where the frequency of a well-watered plant rises and then decreases, as in cluster C6, the fall reflects the growth and developmental dynamics of the stem and must not be read as a stress response. The behavioural classification supports this reading: the nominally stressed plants of cluster C4, whose substrate never actually dried, behave like the irrigated controls, while the single irrigated plant that did dry, P48, behaves like a stressed one. The signal therefore follows the real water status of the plant and not the treatment it was assigned, an observation that also bears on how such experiments should be interpreted, since a nominal treatment is not by itself evidence that the intended stress was imposed.

The weakness of the direct correlation with the vapour pressure deficit reinforces the same point. A frequency merely echoing the daily atmospheric cycle would correlate with the

evaporative demand regardless of treatment; instead, the freq-VPD correlation does not separate the two groups, and only a small residual coupling remains once the soil water potential is held constant. The dominant driver of the signal is the water available at the roots, not the demand of the air, and the two act on different time scales, the soil link residing in the slow drying trend and the atmospheric link in the circadian cycle, as shown by the opposite response of the two correlations to smoothing. This separation is what allows the frequency to be read as a soil-water-stress signal and it distinguishes the signal from indices based on the daily contraction of the stem, such as the maximum daily shrinkage derived from trunk diameter variation, whose interpretation is complicated precisely because they conflate the atmospheric and the soil components of the daily water balance (Zweifel et al., 2001).

Two features give the indicator practical value. First, at the sub-daily scale the frequency leads the soil water potential by about four hours: the stem responds to the evaporative demand ahead of the slower, more buffered soil potential, so the signal carries an early trace of the developing stress. The direction agrees with what is known of the daily water relations of stems, in which the tissue is depleted during the hours of peak transpiration and recovers overnight, ahead of the response of the bulk soil (Zweifel et al., 2001). Second, and more important in practice, the frequency keeps responding in the range where the conventional soil sensor fails. The Watermark potential becomes unreliable beyond about -239 kPa and saturates at the dry end, exactly the range reached under severe deficit, whereas the stem frequency continues to change as the stress deepens. The plant-based signal thus extends the monitoring into the range that matters most for irrigation under deficit, a complementarity taken up in full in Section 5.3.

One further nuance concerns the most severely stressed plants, in which the frequency, after falling with the drying, may rise again in the late stage. This late rise should not be read as a recovery of the plant: a more likely explanation is that beyond a certain level of dehydration the integrity of the tissue begins to fail: the rupture of the cell walls and membranes releases ions into the free space and lowers the electrical impedance of the stem, so that the frequency rises even though the water status is not improving, an effect that may be compounded by cavitation of the water columns in the xylem. This reading is consistent with a long-established observation in plant physiology, that desiccation causes solutes to leak from the cells and raises the electrical conductivity of the tissue, the principle on which the electrolyte-leakage assay of membrane damage is based (Leopold et al., 1981). On this reading the late increase is the signature of an internal damage dynamic. It remains a hypothesis here, coherent with the impedance mechanism and with the leakage literature but not independently verified in this work, and it would need destructive measurements of membrane integrity to be confirmed.

Finally, the relationship, over the range covered here, is described as linear, with a median coefficient of determination of about 0.63 and no advantage from an exponential or a power-law form. This figure is far below the coefficients reported by studies that measure impedance spectra on tissue at controlled water contents, such as the value close to unity obtained by Zhang et al. (2024) on tomato stems across a narrow range of moisture levels, but the two situations are not comparable: those measurements are made at discrete, imposed water contents under controlled conditions, whereas the present coefficients come from a continuous in vivo record in a greenhouse, where the signal also carries the growth of the plant and the daily atmospheric cycle. Seen in that light a coefficient of about 0.6 sustained over weeks of autonomous monitoring is a reasonable performance for the intended purpose. Together with the low-cost, low-power and plant-wearable nature of the sensor, this supports the stem frequency as a practical stress-detection signal. It should be read, however, as a qualitative indicator of the onset and progression of stress rather than as a calibrated measure of tissue water content, and its diagnostic value is confined to the drying phase, since in the well-watered phase the signal is dominated by growth; these limits are discussed in Section 5.4.

5.2 The drainage of gravitational water and the domain of validity of the model

The systematic overestimation of the field-capacity plants (Section 4.3) follows from the structure of the model. In the balance the only loss term is the evapotranspiration: the simulation starts at field capacity and subtracts the daily crop evapotranspiration, so the water content can only decline gradually and regularly, at the rate set by the atmospheric demand and the stress coefficient. The model has no term that removes water quickly, and any water present above field capacity is set to zero at the first step, because the depletion is constrained not to become negative. A rapid early fall of the water content is therefore outside what the balance can produce by construction.

The observed water content behaves differently because the real substrate loses water by two processes at once, evapotranspiration and the gravitational drainage of the water held above field capacity. In the first days after the substrate has been wetted this drainage is rapid and dominant: the excess water moves downward under gravity and leaves the root zone without passing through the plant. Once the gravitational water is exhausted the drainage stops and only the evapotranspiration remains, and from that point the observed and the simulated content follow one another. This is exactly the pattern seen in the data: the discrepancy appears only in the plants that begin above field capacity, it is largest where they begin wettest, and it disappears once the substrate has drained.

This behaviour is coherent with the substrate's hydrological properties. Peat-based growing media are characterised by a high total porosity and by the release of a large fraction of their water over a narrow range of low tension, a behaviour that distinguishes them from agricultural soils and that underlies the classification of an ideal substrate proposed by De Boodt and Verdonck, in which media whose retention curve lies below the ideal range release their water rapidly (Londra et al., 2018; Raviv et al., 2019). Londra et al. (2018) show, for peat-based substrates, that the unsaturated hydraulic conductivity decreases sharply within the range of pressure heads spanned between two successive irrigations, which is to say that the substrate conducts water readily when close to saturation and almost ceases to do so once it has drained. The fitted retention curve of the present substrate has the same character, releasing nearly half of its available water between about -1 and -10 kPa (Section 3.3.1). A substrate of this kind therefore possesses, by construction, a large and rapidly draining gravitational fraction, and it is precisely this fraction that falls outside the balance.

The crop coefficient alone cannot absorb this discrepancy. First, although the whole-series RMSE keeps decreasing as the coefficient is raised beyond the mid-season value, reaching 0.037 for P16 at Kc = 1.30, a coefficient above 1.15 has no physical meaning for tomato: 1.15 is the FAO-56 maximum at full canopy. Second, decomposing the error in time shows that raising the coefficient improves only the tail of the series: the error of the first six days stays at about 0.074 for every coefficient from 1.00 to 1.30, and the share of the total error carried by those first days grows from 31 per cent at Kc = 1.00 to 65 per cent at Kc = 1.30 (Section 4.3). The disagreement is therefore a matter of the shape of the early fall, which the coefficient does not control, and not of its amplitude, which it does. Third, the discrepancy is not distributed as an error in the crop coefficient would be: a coefficient that is too low would produce a proportional and persistent underestimation of the depletion throughout the record, whereas the observed gap is concentrated in the first days and closes afterwards. The observed loss of water over the first days exceeds the simulated evapotranspiration by a factor of 1.75 to 2.67 in the field-capacity plants (Section 4.3), an excess that no admissible evapotranspiration can supply, since closing it would require a crop coefficient of two to three, well beyond the range tabulated for any crop at full canopy. The excess cannot be attributed to the stress coefficient, which is

still at unity in those first days, so the model is already losing water as fast as it can. Nor can it be attributed mainly to the reference evapotranspiration: scaling ET0 within its plausible uncertainty, a factor of about 1.2 to 1.5 compatible with the uncertainty on the cover transmissivity examined in Section 3.3.2, reduces the error but does not reproduce the shape of the fall, and in any case an error in ET0 would act uniformly across a cluster, whereas the gap instead scales with the initial water content of each plant. The one term that accounts for an excess of exactly this form, concentrated in the first days and growing with the initial wetness, is the gravitational drainage.

The drainage in question is that of the gravitational water, the fraction held between saturation and field capacity. This water is retained only weakly, against a tension of the order of a few kilopascals, so that it moves downward under gravity and leaves the root zone in the first days, before the substrate settles at field capacity. Its amount is the difference between the initial content and field capacity, which is largest in the plants that begin near saturation and vanishes in those that begin already within the release range; the size of the omitted term therefore scales with how wet each plant begins, as the mass balance shows. Field capacity marks the end of this phase, the point at which the gravitational water has drained, and evapotranspiration becomes the only remaining outflow.

The omission of gravitational water is a deliberate feature of the FAO-56. The guidelines acknowledge that the drainage and deep percolation terms are difficult to measure and assume that they can be neglected once the profile has drained to field capacity, an assumption that is reasonable in the agricultural soils for which the method was developed and that has been adopted in the many soil water balance studies built on it (Allen et al., 1998). The present results show where that assumption ceases to hold. In a high-porosity growing medium the gravitational fraction is large, its drainage is fast, and a monitoring record that begins while the substrate is still draining therefore covers a period in which the neglected term is the dominant one. The limitation is thus not specific to AgrHyd.

The conclusion is that the simulated and the observed water content are not the same physical quantity during the drainage phase. The simulated content is a reservoir depleted only by the plant, whereas the observed content is the conversion of a potential that responds to any loss of water, the gravitational drainage included. The two coincide once the gravitational water has drained, and this is precisely the region in which the model reproduces the observations, as the close agreement of the plants that begin already dry confirms, with RMSE between 0.003 and 0.012. The water balance is therefore valid in the slow-release zone of the retention curve, where evapotranspiration is the only outflow, and departs from the observations during the rapid drainage that follows saturation. This defines the domain of validity of the model: within that domain, the slow-release region that spans the range relevant to stress, the agreement is close, and the systematic bias of the wet-starting plants is the evidence of a process that lies outside it. In practical terms the model can be used to follow the depletion of a substrate that has already started draining, but its predictions should not be relied upon in the days immediately following saturation, a limitation that matters for greenhouse container systems, where irrigation returns the substrate to saturation frequently.

5.3 The two approaches compared

The two approaches followed in this work describe the same process, a plant progressively depleting the water available to it, from opposite ends of the soil-plant-atmosphere continuum. The water balance reconstructs the water stored in the substrate from the atmospheric demand and the properties of the medium and so describes the supply side of the continuum; the stem

frequency reads the state of the plant tissue and so describes the response side. They are methodologically independent, sharing no parameter and no measurement chain.

The comparison between the stem frequency and the simulated crop evapotranspiration (Section 4.3) shows that the two are positively associated in every plant, but that the association is confined to the phase in which the plant is under deficit: modest over the whole record in the plants that pass through a growth phase first, and high throughout in those already dry at the start of monitoring. The agreement between the two approaches therefore emerges specifically where the water deficit governs both.

The partiality of the correlation is expected, because the two quantities are not measures of the same variable. The frequency assesses the water status of the stem tissue, whereas the simulated evapotranspiration is the water consumed by the plant over the day; the first is a state variable and the second a flux. The two converge under water stress because there the deficit governs both, limiting the transpiration through the stress coefficient and depleting the tissue at the same time, while in a well-watered plant they diverge, since the evapotranspiration follows the atmospheric demand and the tissue stays hydrated. This convergence under stress mirrors, from the modelling side, the selectivity found in the frequency analysis (Section 5.1), and the two independent lines of evidence therefore point to the same conclusion.

The most important outcome of the comparison concerns the limits of the two approaches, which prove to be complementary. The substrate-based description is reliable only within a restricted window. At the wet end it fails during the drainage of the gravitational water, which the balance does not represent (Section 5.2); at the dry end the soil water potential on which the observed content is built becomes unreliable beyond about -239 kPa and saturates thereafter, so the derived water content flattens near the residual value and carries no further information. The window in which the substrate description is trustworthy is thus bounded on both sides, and it is narrow because the retention curve of this substrate releases most of its water over a short interval of potential. The stem frequency has the opposite profile: it is uninformative while the plant is well watered, which is where the balance works best, and it keeps responding as the stress deepens, which is where the soil measurement has already saturated. Each approach is therefore informative in the range where the other is weakest and taken together they cover the drying process more completely than either does alone.

This division of labour matches what is known of the two families of methods in irrigation management. Reviews of irrigation scheduling contrast the traditional water-balance and soil-moisture approaches with those based on sensing the plant response to water deficit, and assign to each a distinct role (Jones, 2004). Soil-based and balance-based methods indicate both when to irrigate and how much water to apply, since they quantify the depletion in depth of water, but they are limited by the spatial variability of the soil and by the difficulty of measuring the terms they neglect; plant-based methods indicate when the plant is suffering, but are hindered by their sensitivity to the atmospheric demand and by a low sensitivity to mild deficits (López-Bernal et al., 2024). The present results reproduce both sides of this description. The balance gives the quantity, converting the depletion into millimetres of water that could be used to size an irrigation; the frequency gives the timing, signalling the onset and the progression of the deficit but saying nothing, for now, about how much water to restore.

The two known weaknesses of plant-based methods also appear here, analysed in Chapter 4. The sensitivity to atmospheric demand was tested directly through the partial correlations: once the vapour pressure deficit is held constant the association between frequency and soil water potential is preserved, and even strengthened, so in this configuration the signal is not a disguised measure of the evaporative demand. The low sensitivity to mild deficits is confirmed, since the frequency is uninformative in the irrigated controls and in the plants of cluster C4,

where a real deficit never developed; this is a genuine limitation, shared by the family of plant-based indicators. It is also the limitation that the balance covers, since the model describes precisely the phase of gradual depletion that precedes the onset of stress.

Read together, the two approaches therefore support an integrated use. A practical monitoring scheme would use the water balance to follow the depletion of an already drained substrate and to quantify the water to be restored, and the stem frequency to detect the moment at which the plant begins to suffer and to continue tracking the deficit once the soil measurement has saturated. The contribution of this work is to have quantified, on the same plants and over the same drying cycles, both the region in which each approach is reliable and the region in which it is not, over a wider set of measurements than the data adopted in previous studies.

5.4 Limitations and future developments

The limited number of plants compared (8) must be considered to interpret the results. The root mean square error is computed over the whole daily series of each plant, but the plants differ in the length of their record and in the number of days over which the substrate is within its release range, where the derived water content actually varies; for the plants that begin already dry this active part of the record is only a few days long. Still, the consistency of the result across plants of different record length and behaviour indicates that the pattern is not an artefact.

The retention curve of the substrate is constrained by measured points only down to -10 kPa, the range characterised in the technical datasheet. The water content at the more negative potentials reached by the stressed plants, and particularly the wilting point adopted as the lower bound of the model, is obtained by extrapolating the fitted curve. No independent measurement is available to confirm the retention behaviour of the substrate in that range.

The observed water content is obtained from a point measurement of soil water potential, taken by an instrument that samples a limited volume of the substrate, through a curve that is steep over the range of interest, so that a small difference in the recorded potential translates into a large difference in the derived water content. The extent to which the probe is representative of the mean water content of the substrate cannot be established with the data available. The soil water potential sensor itself is reliable only down to -239 kPa, beyond which its readings retain their order but may not be precise on their absolute value.

The mass balance establishes that the observed decrease exceeds by a large factor the water that evapotranspiration can account for, and the drainage of gravitational water is the outflow consistent with the magnitude of the excess, with its dependence on the initial water content, and with its disappearance once the substrate has fallen below field capacity. The drainage itself, however, was not measured, and the residual departures observed on the driest plants, where the ratio between observed loss and simulated evapotranspiration falls below unity, are not explained by it and cannot be attributed to a single cause with the data available.

Two measurements would resolve most of these limitations. A gravimetric measurement of the pots, by weighing them at intervals, would give the mean water content directly, and would allow the water leaving the substrate to be separated into the fraction that passes through the plant and the fraction that drains. Collecting and measuring the percolate at the base of the pots would quantify the drainage term explicitly. Either of these would turn the interpretation proposed here into a measured quantity. Extending the retention curve to more negative potentials would remove the reliance on extrapolation, and a second probe placed at a different depth would allow the representativeness of the point measurement to be assessed.

Chapter 6 Conclusions

This work set out to establish how the water status of a greenhouse crop can be followed reliably enough to support efficient irrigation, in a context in which climate change and the growing scarcity of water make the efficient use of irrigation water a priority, in terms of both quantity and timing. The question was addressed on greenhouse-grown tomato plants through two independent approaches, a measurement made on the plant, the electrical impedance of the stem read as a frequency, and a water balance of the root zone simulated with the AgrHyd model, with the aim of determining what each of them can say about the onset and the progression of water stress.

The stem frequency follows the soil water potential closely in the plants subjected to water deprivation, with a median rank correlation of 0.87 that is preserved, and even strengthened, once the atmospheric demand is partialled out, while in the irrigated controls no such association exists. The signal therefore becomes diagnostic when a deficit develops. Over the range examined the relationship is described as linear, and at the sub-daily scale the frequency leads the soil water potential by about four hours.

The water balance reproduced the drying of the substrate accurately for the plants that were already within the release range at the start of monitoring, and overestimated the water content systematically for those that began at field capacity. The crop coefficient could not absorb this discrepancy, since no physically admissible value reproduces the shape of the early fall, and the mass balance showed that the water lost in the first days exceeds the simulated evapotranspiration by a factor of up to about 2.7. The excess corresponds to the drainage of the gravitational water, a term the balance leaves out because it starts at field capacity and removes any excess at once. Simulated and observed water content are therefore two different physical quantities while the substrate is still draining, and they coincide once it has drained, which defines the domain of validity of the model as the slow-release region of the retention curve.

Taken together, the two approaches answer the question from which the work started. The substrate-based description is confined to a narrow window, bounded at the wet end by the drainage the model leaves out and at the dry end by the saturation of the soil water potential sensor, and it is within that window that it quantifies how much water has been depleted. The stem frequency is silent while the plant is well watered, which is where the balance performs best, and keeps responding as the deficit deepens, beyond the range in which the soil measurement remains meaningful, so it is what signals when the plant begins to suffer. The correlation between the frequency and the simulated evapotranspiration confirms this reading, since the two converge specifically in the phase governed by the water deficit. The contribution of this thesis is to have quantified, on the same plants and over the same drying cycles, the region in which each approach is reliable and the region in which it fails, and so to have shown that the integration of a plant-based signal with a soil water balance describes the development of water stress more completely than either of them achieves alone.

These conclusions are bounded by the conditions under which they were obtained. The plants were grown in containers filled with a single peat-based substrate, in one greenhouse and over a limited number of clusters; the number of plants that met the requirements of the water balance

was small; the frequency is a qualitative indicator of the onset and progression of stress, and its readings do not translate into calibrated values of tissue water content; the retention curve was fitted to points taken from the technical datasheet of the substrate, and the reference evapotranspiration rests on parameters taken from the literature. These limits, discussed in Section 5.4, delimit the generality of the results, and they leave the main conclusion intact, since the complementarity of the two approaches follows from the nature of the two measurements and holds independently of the particular conditions of this experiment.

The continuation of this work lies in an experiment designed around the requirements of the two approaches, since most of the uncertainties encountered here originate in data that were collected for a different purpose. A preliminary characterisation of the substrate would allow the retention curve to be built from measured points of the medium actually used, which would remove the reliance on the datasheet and would fix the field capacity and the wilting point on which the whole balance rests. A daily record of the water applied at each irrigation and of the water lost by the end of the day, kept alongside the sensor measurements, would close the balance term by term and would supply the drainage that the model omits, which is the quantity that this work could only estimate indirectly. Extending the model to a sub-daily step would resolve the drying within the day, where the frequency already shows structure that a daily balance cannot follow, and would allow the two descriptions to be compared at the scale at which the plant responds. Together these additions would make it possible to apply AgrHyd more accurately in a container system and to establish more firmly what the electrical impedance of the stem contributes to the monitoring of water status. The contribution of this work is to have quantified, on the same plants and over the same drying cycles, both the region in which each approach is reliable and the region in which it is not, which is what makes their integration more informative than the use of either in isolation.

References

Allen, R.G., Pereira, L.S., Raes, D., Smith, M. (1998). Crop evapotranspiration: guidelines for computing crop water requirements. *FAO Irrigation and Drainage Paper No. 56*. FAO, Rome.

Baille, A. (1999). Overview of greenhouse climate control in the Mediterranean regions. In: Choukr-Allah, R. (ed.), *Protected cultivation in the Mediterranean region*. Cahiers Options Méditerranéennes, n. 31. CIHEAM, Zaragoza, pp. 59-76.

Comparini, D., Masi, E., Pandolfi, C., Sabbatini, L., Dolfi, M., Morosi, S., Mancuso, S. (2020). Stem electrical properties associated with water stress conditions in olive tree. *Agricultural Water Management*, 234, 106109.

Cum, F., Alfarano, L., Pugliese, M., Demarchi, D., Garlando, U. (2024). Preliminary Analysis of Biotic and Abiotic Stress on Tomato Plants Using Impedance Measurements and Time Series Clustering. In: *2024 IEEE Conference on Agrifood Electronics (CAFE)*, Xanthi, Greece, pp. 125-129.

EN 13041:2012. *Soil improvers and growing media, Determination of physical properties , Dry bulk density, air volume, water volume, shrinkage value and total pore space*. European Committee for Standardization, Brussels.

FAO (2021). *The State of the World's Land and Water Resources for Food and Agriculture, Systems at Breaking Point*. Synthesis Report 2021. FAO, Rome.

Fernández, M.D., Bonachela, S., Orgaz, F., Thompson, R.B., López, J.C., Granados, M.R., Gallardo, M., Fereres, E. (2010). Measurement and estimation of plastic greenhouse reference evapotranspiration in a Mediterranean climate. *Irrigation Science*, 28, 497-509.

Garlando, U., Bar-On, L., Ros, P.M., Sanginario, A., Calvo, S., Martina, M., Avni, A., Shacham-Diamand, Y., Demarchi, D. (2021). Analysis of In Vivo Plant Stem Impedance Variations in Relation with External Conditions Daily Cycle. In: *2021 IEEE International Symposium on Circuits and Systems (ISCAS)*, pp. 1-5.

Garlando, U., Calvo, S., Barezzi, M., Sanginario, A., Ros, P.M., Demarchi, D. (2022). Ask the plants directly: understanding plant needs using electrical impedance measurements. *Computers and Electronics in Agriculture*, 193, 106707.

Garlando, U., Calvo, S., Barezzi, M., Sanginario, A., Ros, P.M., Demarchi, D. (2023). A "Plant-Wearable System" for Its Health Monitoring by Intra- and Interplant Communication. *IEEE Transactions on AgriFood Electronics*, 1(2), 60-70.

Hamed, et al. (2023). Towards Tomato Plant Iron Stress Monitoring Through Bioimpedance and Circuit Analysis. In: *2023 IEEE Conference on AgriFood Electronics (CAFE)*, pp. 20-24.

Hargreaves, G.H., Samani, Z.A. (1985). Reference crop evapotranspiration from temperature. *Applied Engineering in Agriculture*, 1(2), 96-99.

Hayden, R.I., Moyse, C.A., Calder, F.W., Crawford, D.P., Fensom, D.S. (1969). Electrical impedance studies on potato and alfalfa tissue. *Journal of Experimental Botany*, 20(2), 177-200.

IPCC (2022). *Climate Change 2022: Impacts, Adaptation and Vulnerability*. Contribution of Working Group II to the Sixth Assessment Report of the Intergovernmental Panel on Climate Change [Pörtner, H.-O., Roberts, D.C. et al. (eds.)]. Cambridge University Press, Cambridge, UK and New York, NY, USA.

Jócsák, I., Végvári, G., Vozáry, E. (2019). Electrical impedance measurement on plants: a review with some insights to other fields. *Theoretical and Experimental Plant Physiology*, 31(3), 359-375.

Jones, H.G. (2004). Irrigation scheduling: advantages and pitfalls of plant-based methods. *Journal of Experimental Botany*, 55(407), 2427-2436.

Leopold, A.C., Musgrave, M.E., Williams, K.M. (1981). Solute leakage resulting from leaf desiccation. *Plant Physiology*, 68(6), 1222-1225.

Li, J., Li, M., Mao, H., Zhu, W. (2016). Diagnosis of potassium nutrition level in *Solanum lycopersicum* based on electrical impedance. *Biosystems Engineering*, 147, 130-138.

Li, J., et al. (2019). Maturity assessment of tomato fruit based on electrical impedance spectroscopy. *International Journal of Agricultural and Biological Engineering*, 12(4), 154-161.

Li, M., Li, J., Mao, H., Wu, Y. (2016). Diagnosis and detection of phosphorus nutrition level for *Solanum lycopersicum* based on electrical impedance spectroscopy. *Biosystems Engineering*, 143, 108-118.

Li, M., et al. (2017). Early diagnosis and monitoring of nitrogen nutrition stress in tomato leaves using electrical impedance spectroscopy. *International Journal of Agricultural and Biological Engineering*, 10(3), 194-205.

Londra, P., Paraskevopoulou, A., Psychogiou, M. (2018). Hydrological behavior of peat- and coir-based substrates and their effect on Begonia growth. *Water*, 10(6), 722.

López-Bernal, Á., García-Tejera, O., Testi, L., Villalobos, F.J. (2024). Irrigation Scheduling Using Plant- and Soil-Based Methods. In: Villalobos, F.J., Fereres, E. (eds), *Principles of Agronomy for Sustainable Agriculture*. Springer, Cham.

Matheny, A.M., Garrity, S.R., Bohrer, G. (2017). The Calibration and Use of Capacitance Sensors to Monitor Stem Water Content in Trees. *Journal of Visualized Experiments*

Orgaz, F., Fernández, M.D., Bonachela, S., Gallardo, M., Fereres, E. (2005). Evapotranspiration of horticultural crops in an unheated plastic greenhouse. *Agricultural Water Management*, 72(2), 81-96.

Raviv, M., Lieth, J.H., Bar-Tal, A. (eds.) (2019). *Soilless Culture: Theory and Practice*, 2nd ed. Academic Press, London.

Rolle, M., Tamea, S., Claps, P. (2021). ERA5-based global assessment of irrigation requirement and validation. *PLoS ONE*, 16(4), e0250979.

Serrano-Finetti, E., Castillo, E., Alejos, S., León Hilario, L.M. (2023). Toward noninvasive monitoring of plant leaf water content by electrical impedance spectroscopy. *Computers and Electronics in Agriculture*, 210, 107907.

Shock, C.C., Barnum, J.M., Seddigh, M. (1998). Calibration of Watermark soil moisture sensors for irrigation management. In: *Proceedings of the International Irrigation Show*, San Diego, CA, 1-3 November 1998. Irrigation Association, pp. 139-146.

Sugiyama, M., Okajima, M. (2022). Application of electrochemical impedance spectroscopy and modeling of the novel equivalent circuit for monitoring cellular tissues. *Theoretical and Experimental Plant Physiology*, 34. https://doi.org/10.1007/s40626-022-00260-2

Taiz, L., Zeiger, E. (2002). *Plant Physiology*, 3rd ed. Sinauer Associates, Sunderland, MA.

Tian, H., Zhao, Y., Gao, C., Xie, T., Zheng, T., Yu, C. (2022). Assessing the Vitality Status of Plants: Using the Correlation between Stem Water Content and External Environmental Stress. *Forests*, 13(8), 1198.

United Nations (2015). *Transforming our World: the 2030 Agenda for Sustainable Development*. Resolution A/RES/70/1. United Nations General Assembly, New York.

van Genuchten, M.Th. (1980). A closed-form equation for predicting the hydraulic conductivity of unsaturated soils. *Soil Science Society of America Journal*, 44(5), 892-898.

Zhang, B., Dong, Z., Sui, X., Gao, J., Feng, L. (2024). Detection of water content in tomato stems by electrical impedance spectroscopy: Preliminary study. *Computers and Electronics in Agriculture*, 219, 108755.

Zhang, M.I.N., Willison, J.H.M. (1993). Electrical impedance analysis in plant tissues: impedance measurement in leaves. *Journal of Experimental Botany*, 44(8), 1369-1375.

Zhang, Y., Chen, Y., Chang, Z., Zhao, J., Wang, X., Xian, J. (2024). Detection of Localized Damage in Tomato Based on Bioelectrical Impedance Spectroscopy. *Agronomy*, 14(8), 1822.

Zhou, J., Wu, S., Chen, J., Sun, B., Di, B., Shan, G., Qian, J. (2025). Electrical Impedance Spectroscopy Reveals Physiological Acclimation in Apple Rootstocks During Recurrent Water Stress Episodes. *Agronomy*, 15(9), 2068.

Zweifel, R., Item, H., Häsler, R. (2001). Link between diurnal stem radius changes and tree water relations. *Tree Physiology*, 21(12-13), 869-877.

Appendices

This appendix collects the code, the complete parameter sets, the detailed computation of the reference evapotranspiration, and the full set of figures supporting the water balance analysis.

Appendix A Code

The scripts below were used to process the outputs of the water balance model and to compare them with the observations. The observed water content is read from the daily-statistics file of each plant; the simulated water content is obtained from the model output as θ_sim = WCrz + θ_wp.

A.1 Root mean square error over all plants

Computes RMSE, bias and MAE between simulated and observed water content over the whole daily series of each plant, excluding only the anomalous rises of the observed record (sensor artefacts).

```
% RMSE, bias, MAE over the whole series - all plants
theta_wp = 0.299;
W = struct();
% Paste the simulated WCrz series (Kc = 1.15) of each plant:
% W.P16 = [ ... ]; W.P80 = [ ... ]; etc.

plants = fieldnames(W);
for k = 1:numel(plants)
    name = plants{k}; wcrz = W.(name)(:);
    if isempty(wcrz), continue; end
    ID = str2double(erase(name,'P'));
    fn = sprintf('dataset_ID_%d_dailyStats.xlsx', ID);
    if ~isfile(fn), fn = sprintf('dataset_ID_%d_dailyStats.csv', ID); end
    T = readtable(fn);
    theta_obs = T.DailyMean_StemFreq;  % <-- verificare nome colonna theta
    theta_obs = theta_obs(~isnan(theta_obs));
    theta_sim = wcrz + theta_wp;
    n = min(numel(theta_obs), numel(theta_sim));
    theta_obs = theta_obs(1:n); theta_sim = theta_sim(1:n);
    rising = [false; diff(theta_obs) > 0.005];
    valid = ~rising;
    resid = theta_sim(valid) - theta_obs(valid);
    rmse = sqrt(mean(resid.^2));
    bias = mean(resid); mae = mean(abs(resid));
    fprintf('%s: RMSE=%.4f bias=%+.4f MAE=%.4f\n', name, rmse, bias, mae);
end
```

A.2 Retention curve fitting (van Genuchten)

Fits the van Genuchten model to the four points derived from the datasheet, and returns the parameters used to convert the measured potential into water content.

```
% four points from the datasheet
pF_data    = [0, 1, 1.7, 2];
theta_data = [0.90, 0.62, 0.37, 0.33];
theta_s = 0.90;

% van Genuchten: p(1)=alpha, p(2)=n, p(3)=theta_r
vg = @(p,pF) p(3) + (theta_s - p(3)) .* ...
     (1 + (p(1)*10.^pF).^p(2)).^(-(1 - 1./p(2)));
```

```
p0 = [0.5, 2.0, 0.1];
lb = [0.001, 1.1, 0]; ub = [10, 10, 0.4];
p_opt = lsqcurvefit(vg, p0, pF_data, theta_data, lb, ub);

alpha = p_opt(1); n = p_opt(2); theta_r = p_opt(3);
fprintf('alpha=%.4f  n=%.3f  theta_r=%.4f\n', alpha, n, theta_r);

% water content at any potential (SWP in kPa):
% pF = log10(|SWP| * 10.2);  theta = vg(p_opt, pF)
```

A.3 Simulated versus observed water content (single plant)

Plots the observed and simulated water content of a single plant, with the field capacity and wilting point marked, and reports RMSE and bias computed over the whole series.

```
ID = 16;   % change to the plant of interest
WCrz = [ ... ]';   % simulated WCrz (Kc = 1.15) of the plant
theta_wp = 0.299; theta_fc = 0.620;

fn = sprintf('dataset_ID_%d_dailyStats.xlsx', ID);
if ~isfile(fn), fn = sprintf('dataset_ID_%d_dailyStats.csv', ID); end
T = readtable(fn);
theta_obs = T.DailyMean_Theta / 100;   % verificare nome/scala
theta_obs = theta_obs(~isnan(theta_obs));
theta_sim = WCrz + theta_wp;
n = min(numel(theta_obs), numel(theta_sim));
theta_obs = theta_obs(1:n); theta_sim = theta_sim(1:n);
days = (0:n-1)';

rising = [false; diff(theta_obs) > 0.005]; valid = ~rising;
resid = theta_sim(valid) - theta_obs(valid);
rmse = sqrt(mean(resid.^2)); bias = mean(resid);

figure('Color','w'); hold on;
yline(theta_fc,'--','Field capacity','Color',[0.4 0.4 0.4], ...
    'LabelHorizontalAlignment','left');
yline(theta_wp,'--','Wilting point','Color',[0.4 0.4 0.4], ...
    'LabelHorizontalAlignment','left');
plot(days, theta_obs,'-o','Color',[0.20 0.35 0.65],'LineWidth',1.6, ...
    'MarkerFaceColor',[0.20 0.35 0.65],'DisplayName','Observed');
plot(days, theta_sim,'-s','Color',[0.80 0.33 0.20],'LineWidth',1.6, ...
    'MarkerFaceColor',[0.80 0.33 0.20],'DisplayName','Simulated (AgrHyd)');
grid on; xlabel('Days from start of monitoring');
ylabel('Volumetric water content (m^3 m^{-3})');
title(sprintf('Plant %d (RMSE = %.3f, bias = %+.3f)', ID, rmse, bias));
legend('Location','northeast');
```

A.4 Water content for different crop coefficients

Overlays the observed water content with the simulations obtained for the different crop coefficients tested, with the RMSE of each in the legend.

```
theta_wp = 0.299; theta_fc = 0.620;
% observed series of the plant (percentage / 100):
theta_obs = [ ... ]' / 100;
n = numel(theta_obs); days = (0:n-1)';

% one WCrz series per configuration:
WCrz.const115 = [ ... ]; WCrz.const120 = [ ... ];
WCrz.const130 = [ ... ]; WCrz.rampFAO = [ ... ];
```

```
configs = fieldnames(WCrz);
labels = {'K_c = 1.15','K_c = 1.20','K_c = 1.30','FAO ramp + plateau'};
cols = lines(numel(configs));
rising = [false; diff(theta_obs) > 0.005]; valid = ~rising;

figure('Color','w'); hold on;
yline(theta_fc,'--','Field capacity','Color',[0.4 0.4 0.4], ...
    'LabelHorizontalAlignment','left');
yline(theta_wp,'--','Wilting point','Color',[0.4 0.4 0.4], ...
    'LabelHorizontalAlignment','left');
plot(days, theta_obs,'-o','Color','k','LineWidth',2.4, ...
    'MarkerFaceColor','k','DisplayName','Observed');
for i = 1:numel(configs)
    w = WCrz.(configs{i})(:); ts = w + theta_wp;
    m = min(numel(ts), n); resid = ts(1:m) - theta_obs(1:m);
    rmse = sqrt(mean(resid(valid(1:m)).^2));
    lbl = sprintf('%s  (RMSE = %.3f)', labels{i}, rmse);
    plot(days(1:m), ts(1:m), '-','Color',cols(i,:),'LineWidth',1.5, ...
        'DisplayName',lbl);
end
grid on; xlabel('Days from start of monitoring');
ylabel('Volumetric water content (m^3 m^{-3})');
legend('Location','northeast');
```

A.5 Stem frequency versus simulated evapotranspiration

Compares the daily mean stem frequency with the simulated crop evapotranspiration, both normalised, and reports the Spearman correlation. For the plants of C2 the coefficient is computed over the stress phase (after the split); for those of C7, over the whole series.

```
ID = 16;
% frequency (daily mean) from the plant file:
ffile = sprintf('dataset_ID_%d_dailyStats.xlsx', ID);
if ~isfile(ffile), ffile = sprintf('dataset_ID_%d_dailyStats.csv', ID); end
F = readtable(ffile); freq = F.DailyMean_StemFreq;
% simulated ET from the model output:
E = readtable(sprintf('P%d_tomato_results_2024_2024_FINAL.csv', ID));
etc = E.ET;

n = min(numel(freq), numel(etc));
freq = freq(1:n); etc = etc(1:n); days = (0:n-1)';
ok = ~isnan(freq) & ~isnan(etc);

fn = (freq - min(freq)) / (max(freq) - min(freq));
en = (etc  - min(etc))  / (max(etc)  - min(etc));

figure('Color','w'); hold on;
plot(days, fn, '-o','LineWidth',1.8,'Color',[0 0.2 0.6], ...
    'DisplayName','Stem frequency');
plot(days, en, '-s','LineWidth',1.8,'Color',[0.75 0.2 0.1], ...
    'DisplayName','Simulated ET_c');
xlabel('Days from start of monitoring');
ylabel('Normalised value (0-1)'); legend('Location','best'); grid on;

% Spearman: intera serie (C7) o fase stress (C2, dallo split)
rho_all = corr(freq(ok), etc(ok), 'Type','Spearman');
% split = 14;  late = (days >= split) & ok;
% rho_late = corr(freq(late), etc(late), 'Type','Spearman');
fprintf('Plant %d: Spearman = %.3f\n', ID, rho_all);
```

Appendix B Model parameters and crop coefficient grid

B.1 Substrate and model parameters

Table B.1. Van Genuchten parameters of the substrate and characteristic water contents.

Parameter	Symbol	Value
Saturated water content	θs	0.90
Residual water content	θr	0.299
Field capacity (−1 kPa)	θfc	0.62
Wilting point (−1500 kPa)	θwp	0.299
Shape parameter	α	0.151 cm^{-1}
Shape parameter	n	2.068
Shape parameter	m = 1 − 1/n	0.516

The fit reproduces the four datasheet points with an RMSE of 0.003; the residual water content coincides with the wilting point extrapolated to −1500 kPa.

Table B.2. Model configuration used for the simulations.

Parameter	Value
Rooting depth Zr	0.14 m (constant)
Depletion factor DF (p)	0.40
Total available water TAW	44.9 mm
Readily available water RAW	18.0 mm
Crop coefficient Kc	1.15 (constant)
Water input (P, I)	0

B.2 Complete crop coefficient grid

The crop coefficient was explored over both constant and ramped forms, and beyond the mid-season value, for the two reference plants. RMSE over the whole daily series.

Table B.3. RMSE between simulated and observed water content for the crop coefficients tested (P16 and P80).

Kc configuration	P16	P80
ramp 0.80 → 0.90	0.101	0.140
constant 1.00	0.053	0.116
ramp 1.00 → 1.15	0.051	0.116
FAO ramp + plateau	0.049	0.060
constant 1.15	0.042	0.039
constant 1.20	0.041	0.044
constant 1.30	0.037	0.040

B.3 Initial conditions of the plants

Table B.4. Initial water content and initial available water (ini_sm) for each plant. Plants above field capacity use ini_sm = null (the model initialises at field capacity).

Plant	Cluster	θ day 1	ini_sm
P80	C7	0.765	null
P18	C2	0.750	null
P19	C2	0.749	null
P16	C2	0.712	null
P81	C7	0.392	0.093
P79	C7	0.382	0.083
P17	C2	0.363	0.064
P82	C7	0.345	0.046

Appendix C Reference evapotranspiration

The reference evapotranspiration was computed with the FAO-56 Penman-Monteith equation adapted to the greenhouse environment. The global solar radiation was measured by ARPA and attenuated by the greenhouse cover; temperature and relative humidity were measured inside the greenhouse.

Table C.1. Parameters used in the greenhouse reference evapotranspiration.

Parameter	Symbol	Value
Cover transmissivity	τ	0.70
Crop albedo	α	0.23
Internal wind speed	u2	0.3 m s^{-1}
Soil heat flux	G	0
Altitude	z	293 m

C.1 Computation steps

The saturation vapour pressure is obtained from the daily maximum and minimum temperature, and the actual vapour pressure from the relative humidity (Allen et al., 1998):

```
e°(T) = 0.6108 · exp(17.27·T / (T+237.3))
es = (e°(Tmax) + e°(Tmin)) / 2
ea = es · RH/100
```

The net shortwave radiation uses the radiation transmitted through the cover; the net longwave radiation follows the FAO-56 formulation, with the cloudiness term based on the ratio of measured to clear-sky radiation:

```
Rs_in = τ · Rs_out          (radiation inside the greenhouse)
Rns   = (1 - α) · Rs_in
Rso   = (0.75 + 2e-5·z) · Ra    (clear-sky radiation)
Rnl   = σ · (Tmax_K^4 + Tmin_K^4)/2 · (0.34 - 0.14·√ea) · f
  with f = 1.35·(Rs_in/Rso_in) - 0.35
```

```
Rn    = Rns - Rnl
```

The reference evapotranspiration follows the FAO-56 Penman-Monteith equation, with the psychrometric constant from the local atmospheric pressure and the soil heat flux set to zero at the daily step:

$$\Delta = 4098 \cdot e^{\circ}(T_{mean}) / (T_{mean}+237.3)^2$$
$$P = 101.3 \cdot ((293 - 0.0065 \cdot z)/293)^{5.26}$$
$$\gamma = 0.000665 \cdot P$$
$$ET_0 = \frac{0.408 \cdot \Delta \cdot (R_n - G) + \gamma \cdot (900/(T_{mean}+273)) \cdot u_2 \cdot (e_s - e_a)}{\Delta + \gamma \cdot (1 + 0.34 \cdot u_2)}$$

The resulting reference evapotranspiration ranges between about 0.6 and 4.6 mm per day over the monitoring periods. The Hargreaves-Samani estimate was computed alongside for comparison but was not used in the water balance.

C.2 Code

```
% greenhouse parameters
z = 293; tau = 0.7; alpha = 0.23; G = 0; u2 = 0.3;

% vapour pressure
eTmax = 0.6108*exp(17.27*Tmax./(Tmax+237.3));
eTmin = 0.6108*exp(17.27*Tmin./(Tmin+237.3));
es = (eTmax+eTmin)/2;  ea = es.*(RH/100);

% radiation (Rs_out measured by ARPA, Ra extraterrestrial)
Rso   = (0.75 + 2e-5*z).*Ra;
Rs_in = tau.*Rs_out;
Rns   = (1-alpha).*Rs_in;
sigma = 4.903e-9;
Tmax_K = Tmax+273.16; Tmin_K = Tmin+273.16;
cloud = 1.35*(Rs_in./(tau.*Rso)) - 0.35;
cloud = max(0.05, min(1, cloud));
Rnl = sigma*((Tmax_K.^4+Tmin_K.^4)/2).*(0.34-0.14*sqrt(ea)).*cloud;
Rn  = Rns - Rnl;

% Penman-Monteith FAO-56
Delta = 4098*(0.6108*exp(17.27*Tmean./(Tmean+237.3))./(Tmean+237.3).^2;
P = 101.3*((293-0.0065*z)/293)^5.26;  gamma = 0.000665*P;
ET0 = (0.408*Delta.*(Rn-G) + gamma.*(900./(Tmean+273)).*u2.*(es-ea)) ...
      ./ (Delta + gamma.*(1+0.34*u2));
ET0 = max(ET0, 0);
```

Appendix D Simulated versus observed water content, all plants

The figures below show the observed and simulated water content for each of the eight plants, with the field capacity and wilting point marked. They confirm that the pattern described in the main text shows a systematic positive departure for the plants that begin at field capacity, and close agreement for those that begin already dry, and it holds across the whole set.

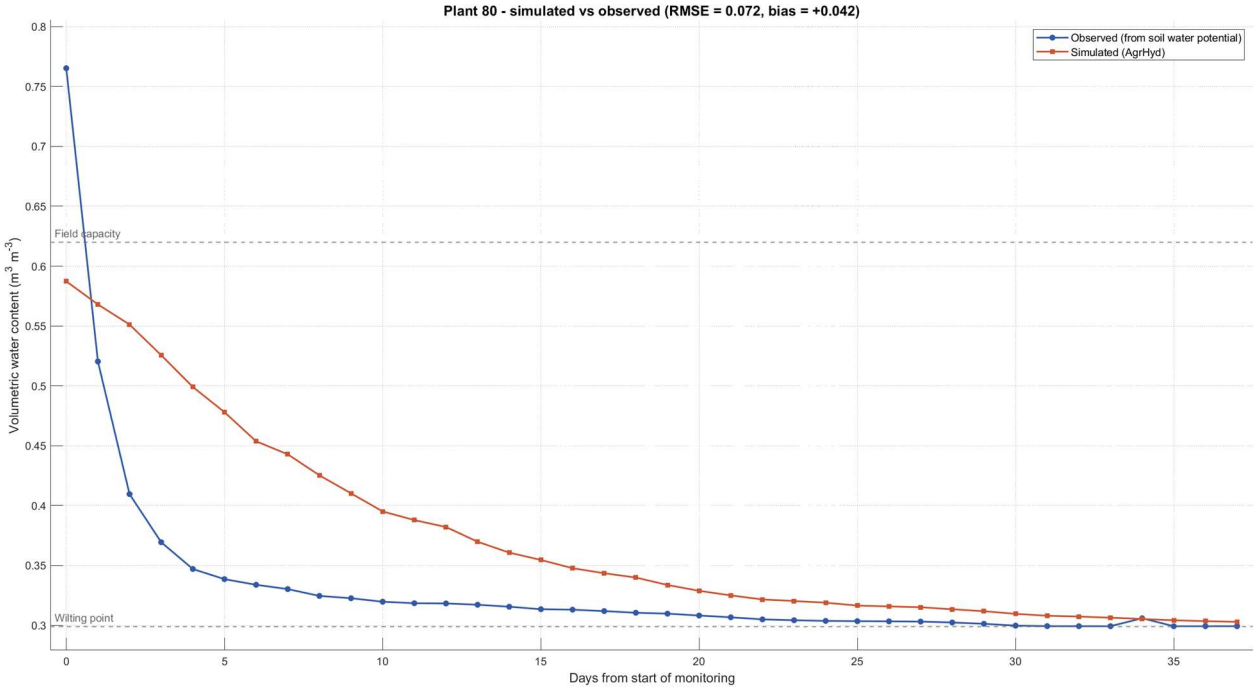


Figure D.1. Observed and simulated water content, P80 (field capacity).

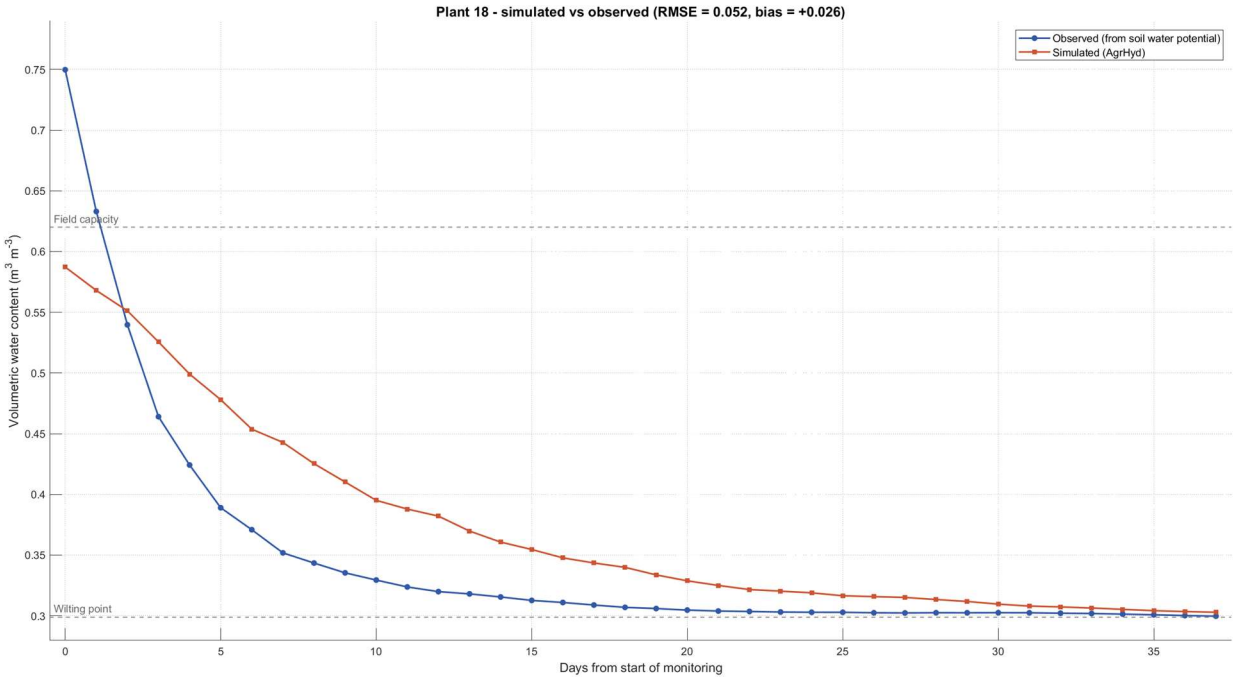


Figure D.2. Observed and simulated water content, P18 (field capacity).

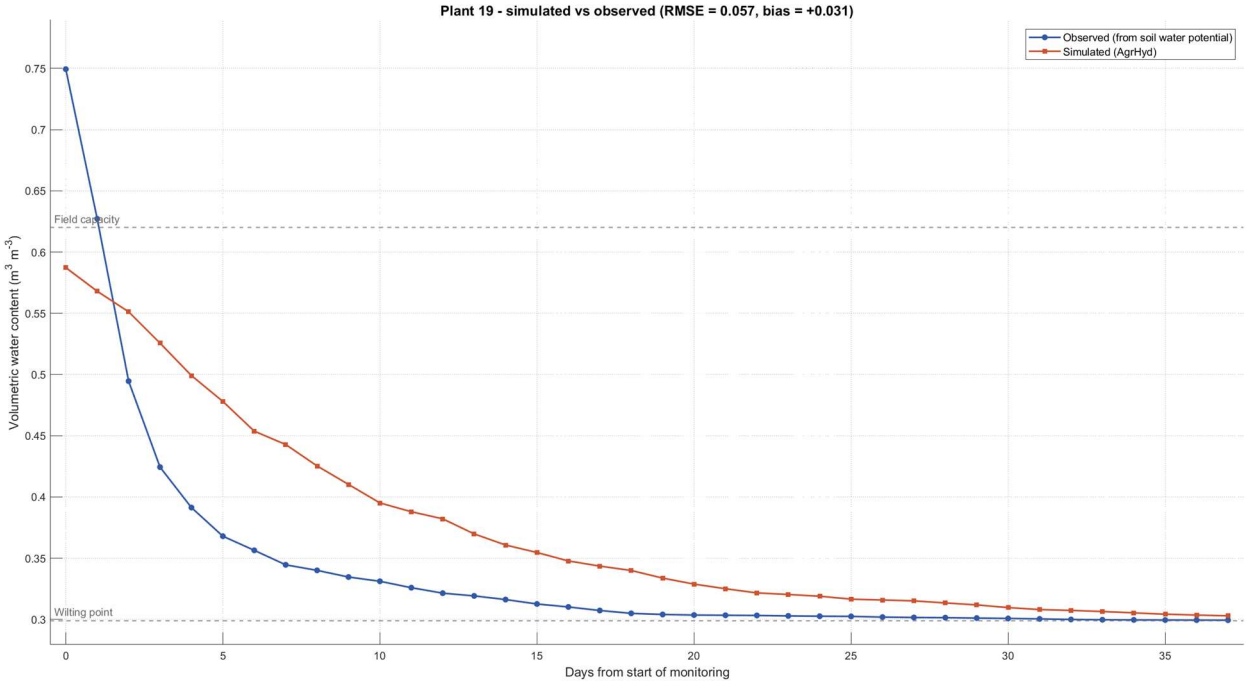


Figure D.3. Observed and simulated water content, P19 (field capacity).

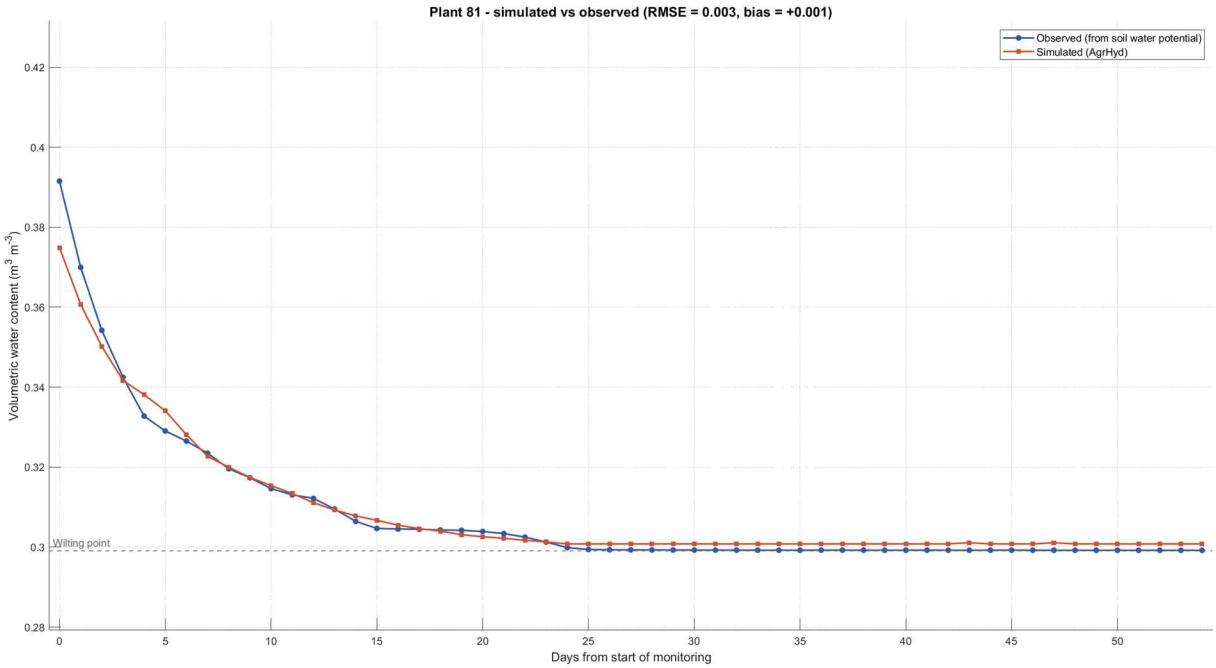


Figure D.4. Observed and simulated water content, P81 (dry).

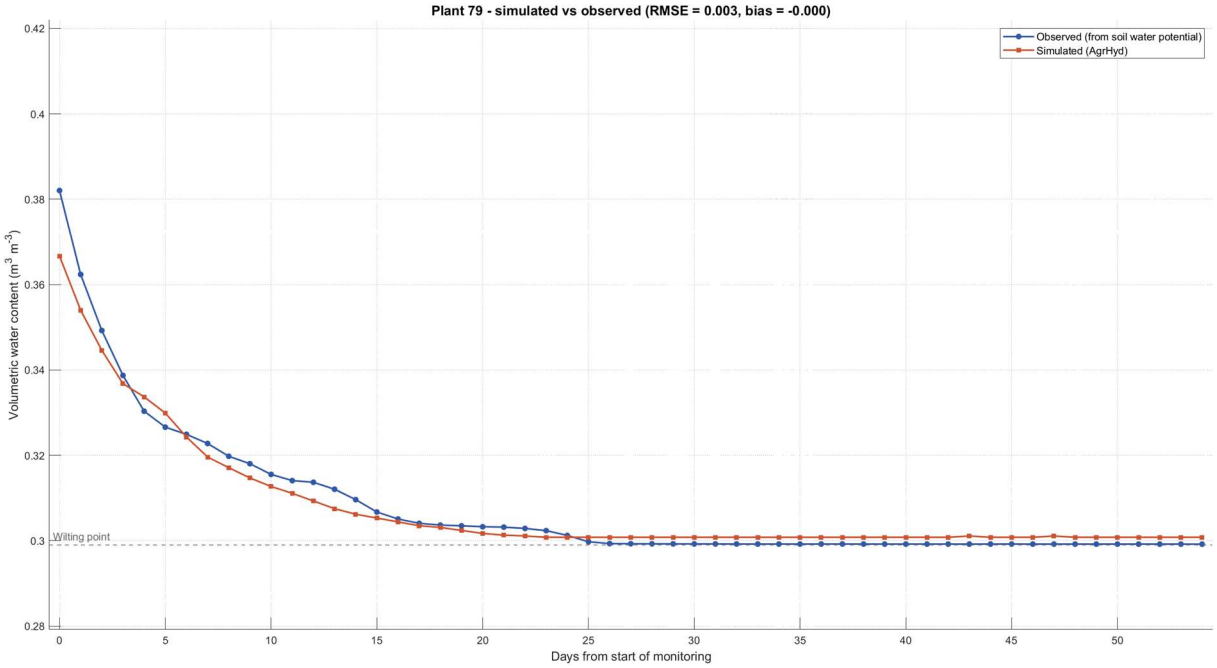


Figure D.5. Observed and simulated water content, P79 (dry).

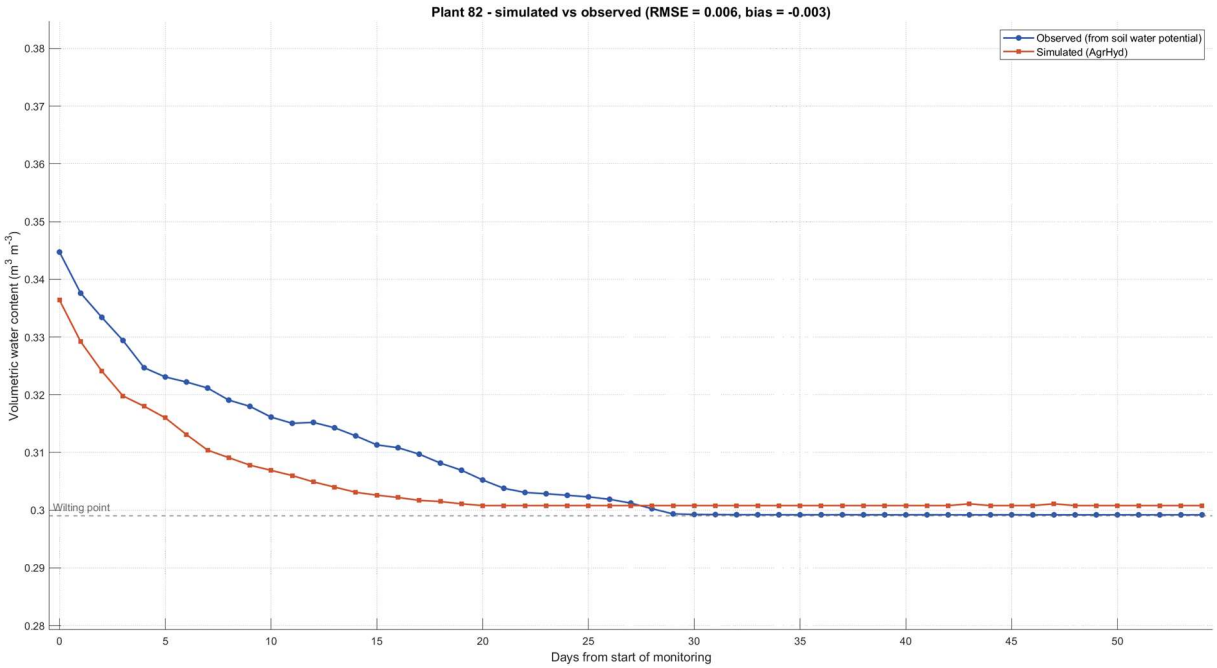


Figure D.6. Observed and simulated water content, P82 (dry).

Acknowledgements

I would like to express my sincere gratitude to my supervisor, Prof. Stefania Tamea and my co-supervisors, Prof. Danilo Demarchi, Amirarsalan Shahmohammadi and Federico Cum, whose expertise and constructive criticism shaped this research at every stage.

I would also like to extend my special thanks to Prof. Claudio Oggeri, whose kindness and empathy were an invaluable source of support at a crucial point in my academic path, encouraging me to continue my studies.

Finally, and most importantly, I wish to thank my family, whose love and support have been with me from the very beginning of this journey. They are, to me, the greatest example of perseverance, resilience, and humility, which has shaped the way I approached the path that led me here.